HHS Public Access

Author manuscript

Cell Rep. Author manuscript; available in PMC 2025 March 20.

Published in final edited form as:

Cell Rep. 2025 February 25; 44(2): 115237. doi:10.1016/j.celrep.2025.115237.

G3BP1 ribonucleoprotein complexes regulate focal adhesion protein mobility and cell migration

Liana C. Boraas[1,2,8,*], **Mengwei Hu**[2,8], **Pieter Martino**[1,2], **Lauren Thornton**[1,2], **Charles E. Vejnar**[2], **Gang Zhen**[3], **Longhui Zeng**[4,5], **Dylan M. Parker**[6], **Andy L. Cox**[2], **Antonio J. Giraldez**[2], **Xiaolei Su**[4,5], **Christine Mayr**[7], **Siyuan Wang**[2,4,*], **Stefania Nicoli**[1,2,9,*]

[1]Yale Cardiovascular Research Center, Department of Internal Medicine, Section of Cardiology, Yale University School of Medicine, New Haven, CT 06511, USA

[2]Department of Genetics, Yale University School of Medicine, New Haven, CT 06510, USA

[3]Laboratory of Genome Integrity, National Cancer Institute, NIH, Bethesda, MD 20892, USA

[4]Department of Cell Biology, Yale University School of Medicine, New Haven, CT 06510, USA

[5]Yale Cancer Center, Yale University, New Haven, CT, USA

[6]Department of Biochemistry and Howard Hughes Medical Institute, University of Colorado Boulder, Boulder, CO, USA

[7]Cancer Biology and Genetics Program, Memorial Sloan Kettering Cancer Center, New York, NY, USA

SUMMARY

The subcellular localization of mRNAs plays a pivotal role in biological processes, including cell migration. For instance, β-actin mRNA and its associated RNA-binding protein (RBP), ZBP1/IGF2BP1, are recruited to focal adhesions (FAs) to support localized β-actin synthesis, crucial for cell migration. However, whether other mRNAs and RBPs also localize at FAs remains unclear. Here, we identify hundreds of mRNAs that are enriched at FAs (FA-mRNAs). FA-mRNAs share characteristics with stress granule (SG) mRNAs and are found in ribonucleoprotein (RNP) complexes with the SG RBP. Mechanistically, G3BP1 binds to FA proteins in an RNA-dependent manner, and its RNA-binding and dimerization domains, essential for G3BP1 to form RNPs in

[*]Correspondence: liana.boraas@yale.edu (L.C.B.), siyuan.wang@yale.edu (S.W.), stefania.nicoli@yale.edu (S.N.).

[8]These authors contributed equally

[9]Lead contact

AUTHOR CONTRIBUTIONS

L.C.B. contributed to all the experiments in the paper and the analysis of the data. M.H. performed experiments, including all MERFISH experiments and data analysis. P.M. contributed to cloning, FRAP, and data analysis. C.E.V. performed the bioinformatic analysis of the poly(A)RNA-seq and Ribo-seq data with guidance from A.J.G. L.Z. and X.S. provided equipment, training, and guidance on the FRAP experiments. D.M.P. provided the GFP-G3BP1 protein for the *in vitro* reconstitution. G.Z. performed the analysis of mRNA properties, and C.M. provided guidance on the direction of the manuscript. S.W. contributed MERFISH-related expertise. L.C.B., S.N., and A.L.C. wrote the paper.

DECLARATION OF INTERESTS

S.W. is a co-inventor on a patent applied for by Harvard University related to the MERFISH technology. S.W. is a shareholder and consultant of Translura, Inc. M.H. is a current employee of Merck Research Laboratories.

SUPPLEMENTAL INFORMATION

Supplemental information can be found online at https://doi.org/10.1016/j.celrep.2025.115237.

SG, are required for FA localization and cell migration. We find that G3BP1 RNPs promote cell speed by enhancing FA protein mobility and FA size. These findings suggest a previously unappreciated role for G3BP1 RNPs in regulating FA function under non-stress conditions.

In brief

Boraas et al. identify that mRNAs and the stress granule RNA-binding protein G3BP1 form ribonucleoprotein (RNP) complexes at FAs. These RNPs regulate FA protein mobility and cell migration under normal conditions. This discovery highlights a role for G3BP1 RNPs in non-stress cellular processes.

Graphical Abstract

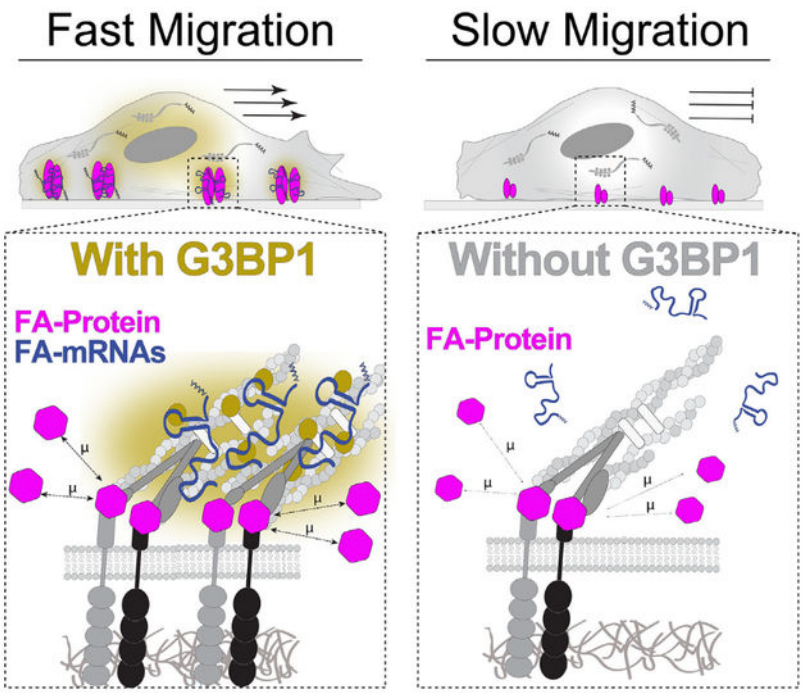

INTRODUCTION

Cell migration is fundamental to many biological processes, including development, wound healing, and immune defense, as well as pathological conditions such as tumor metastasis.[1] Focal adhesions (FAs) mediate cell migration by physically connecting the actin cytoskeleton to integrins, which in turn bind to the surrounding extracellular matrix.[2–4] Paxillin (PXN), vinculin, talin, α-actinin, and many other proteins form layered structures at FAs that are crucial for their function.[5] FAs assemble and disassemble during cell movement, and their size is determined by protein exchange between the FA and cytoplasm.[6,7] These FA dynamics allow the cell to bind to the matrix, pull the cell body

forward, and release.[8,9] Nevertheless, the molecular mechanisms controlling the mobility of FA proteins are poorly understood.

β-actin mRNA (*ACTB*) is a highly abundant cytoplasmic mRNA that also localizes at FAs, and its local translation is important for the formation of stable FAs and cell migration.[10–15] Other mRNAs, while not localized at FAs, accumulate at the leading edge to regulate cell migration through similar mechanisms of local translation or co-translation.[10,15–23] For example, the mRNA *NET1* is poorly translated in the perinuclear side but highly translated in the peripheral side of an adherent cell to regulate local NET1 protein binding, which is key for its function in cell migration.[24] However, a comprehensive understanding of the scope and potential roles of mRNA localization to FAs is unknown.

To fill this knowledge gap, we used an unbiased approach to identify mRNAs and RNA-binding proteins (RBPs) enriched at FAs in normal adherent cells. We detected hundreds of mRNAs and the stress granule (SG) RBP G3BP1 enriched at FAs in unstressed cells. These FA-associated mRNAs (FA-mRNAs) share characteristics with SG mRNAs and form ribonucleoprotein (RNP) complexes with G3BP1 both *in vitro* and *in cellulo*. Mechanistically, the RNA-binding domain (RBD) and dimerization domain of G3BP1, essential for G3BP1 to form RNPs in SGs,[25] are also required for its localization to FA and regulation of cell migration speed. We propose that G3BP1 RNPs do not influence translation but rather promote the mobility of FA proteins, thereby affecting adhesion size, a key feature in regulating cell speed.

RESULTS

A subset of mRNAs is localized at FAs

To comprehensively investigate mRNA enrichment at FAs in adherent cells, we employed an unbiased approach to isolate FA-mRNAs. Using a hydromechanical isolation method,[26] we captured FAs of varying size from whole cells (Figures 1A and 1B; Figures S1A–S1C). We performed these experiments with human dermal fibroblasts (HDFs) and human umbilical vein endothelial cells (HUVECs),[27,28] two common adherent and migratory cell types.

We identified 236 mRNAs in HUVEC FAs and 119 mRNAs in HDF FAs that were enriched by 1.4- to 8.7-fold compared to whole cells ($p$adj < 0.01 [adjusted p value]) (Figure 1C; Figure S1D). Fifty-seven of these mRNAs were enriched at FAs in both cell types (Table S1). As expected, we detected *ACTB* mRNA in our isolated FA samples. However, *ACTB* was not enriched at FAs compared to whole-cell lysates ($p$adj = 0.8738 HDFs, $p$adj = 0.9939 HUVECs), consistent with its high abundance in the cytoplasm (Table S1).

To test the specificity of our approach, we treated cells with blebbistatin (Blebb)[29] for 30 min to disrupt FAs and compared these cells to DMSO-treated and whole-cell samples. FA-mRNA enrichment was observed only in FA isolates from DMSO-treated control cells and not in the Blebb-treated HDFs (Figure 1D). We also introduced an mRNA encoding iRFP (near-infrared fluorescent protein) and found that *iRFP* mRNA was not enriched at FAs under any condition. This finding validates that the observed mRNA enrichment at FAs is not an artifact of the FA isolation method (Figure 1D).

To further validate the subcellular localization of FA-mRNAs, we used single-molecule fluorescent *in situ* hybridization (smFISH) to detect 13 FA-mRNAs in HDFs. As negative controls, we examined *SPKN1* and *KPNA4* mRNAs, which were expressed in our cells but not enriched in isolated FAs (Table S1). FA spatial enrichment was calculated as the ratio of individual mRNA foci co-localizing with FAs, marked with the core FA protein PXN, over the rest of the foci in the cell[30,31] (see STAR Methods). *SPKN1* and *KPNA4* rarely co-localized with PXN and had a negative spatial enrichment to FAs, as expected (Figures 1E and 1F). In contrast, all 13 FA-mRNAs significantly co-localized with FAs, displaying an average of 1.8-fold spatial enrichment at FAs (Figures 1E and 1F).

As an orthogonal approach, we employed multiplexed error-robust FISH (MERFISH)[32] and designed a library of oligonucleotide probes to visualize 122 FA-mRNAs. These FA-mRNAs were selected based on probe accessibility criteria[33] (see STAR Methods; Table S2). As negative controls, we designed a library of probes to capture 136 mRNAs that include (1) 46 mRNAs found at different cellular compartments (e.g., mitochondria, endoplasmic reticulum, cell protrusion, and cytosol),[34] (2) 86 mRNAs not found at FAs but encoding FA proteins,[35,36] and (3) 4 mRNAs found in TIS granules[37,38] (Table S2). Both libraries produced high-quality images, and the number of mRNA foci per cell correlated with RNA sequencing results from whole cells (Figure 1G; Figures S1E and S1F). FA enrichment did not correlate with the overall mRNA abundance in HDFs (Figure S1G). On average, FA-mRNAs were spatially enriched (1.87-fold, $p < 0.0001$) at PXN-positive FAs as determined by MERFISH. In contrast, negative control mRNAs, including those previously detected in cell protrusions that may be randomly proximal to FAs (Figure 1H), did not exhibit FA enrichment. Specifically, 96% of FA-mRNAs were more enriched at FAs than 95% of the control mRNAs, and the two distributions were negatively correlated (Pearson $r = -0.816$, $p = 0.004$). These trends remained consistent even when we compared FA-mRNA with a simulated randomized distribution of mRNAs in whole cells (see STAR Methods; Figures 1H and 1I; Figures S1H and S1I). Collectively, these data support that a subset of mRNAs is spatially enriched at FAs.

The SG protein G3BP1 displays RNA-dependent localization to FAs in unstressed cells

ACTB localization at FAs requires the RBP ZBP1/IGF2BP1[10]; however, FA-mRNA sequences do not contain the ZBP1/IGF2BP1 RNA-binding motif, as determined by HOMER motif analysis[39] (see STAR Methods). To uncover other RBPs with RNA-dependent enrichment at FAs, we performed a proteomics analysis of FA isolates from untreated HDFs and HDFs that were treated with RNase A for 10 min to degrade RNA (Figure 2A; Table S3). Despite acute RNA depletion, HDFs maintained FAs as well as the levels of core FA proteins (VCL, PXN, TLN1, and ACTN1) (Figures S2A–S2D). Interestingly, we identified the canonical SG nucleating protein G3BP1[25,40] among the FA RBPs in FA isolates from untreated HDFs, while its levels were significantly reduced following RNase A treatment (Figure 2B; Figure S2E). G3BP2, a close relative of G3BP1 in SG formation,[25,41] was also found at FAs (Figures S2E and S2F).

To validate our findings, we visualized G3BP1 and G3BP2 alongside PXN. Both proteins localized to the cytoplasm and FA-enriched lamellipodia (Figure 2C; Figures S2G and

S2H). G3BP1 and G3BP2 displayed elevated co-localization to FAs when compared to iRFP, which was instead randomly distributed (Figures 2C and 2D; Figures S2G and S2H), supporting the specificity of their localization. Additionally, in line with the proteomic analysis, a 10-min RNase A treatment of HDFs was sufficient to reduce the G3BP1 enrichment but did not affect iRFP levels at FAs (Figures 2C and 2D).

G3BP1 concentrates to form SGs during cytotoxic stress under, for example, sodium arsenite treatment.[25] However, we did not observe SG formation in untreated HDFs or HDFs treated with RNase A or Blebb (Figure 1E). In contrast, a 30-min sodium arsenite treatment altered G3BP1 localization, causing it to accumulate at SGs but not at FAs (Figures 1E and 1F). We infer that G3BP1 localizes at FAs under non-stress conditions.

To determine if G3BP1 interacts with FA proteins in non-stressed cells, we performed co-immunoprecipitation followed by liquid chromatography-mass spectrometry in HDF (Figure 2G). We evaluated G3BP1-interacting proteins in untreated HDFs and HDFs that were treated with RNase A (10 min) or Blebb (30 min) (Figure 2G). Notably, in non-stressed cells, G3BP1 co-immunoprecipitated with several SG proteins,[42] FA proteins, and cytoskeletal proteins,[35] and the majority of these interactions were lost in HDFs lacking RNA or FAs (Figure 2H; Figures S2I and S2J; Table S4). We validated the reciprocal interaction of G3BP1 with the FA proteins TLN1[43] or ACTN1[44] in untreated cells. These interactions were disrupted by Blebb and RNase A treatment in HDFs (Figure 2I).

Thus, in non-stressed cells, G3BP1 displays RNA-dependent interactions with FAs, SG proteins, cytoskeletal proteins, and FA proteins.

G3BP1 forms RNP complexes with focal-adhesion-associated mRNAs

At SGs, G3BP1 binds to mRNAs that tend to be long and poorly translated, containing AU-rich elements.[42,45,46] Notably, FA-mRNAs were also significantly longer, had a higher AU content, and contained more AU-rich elements than mRNAs that were non-enriched at FAs (Figure S3A). Proteomic analysis of FA isolates revealed that only 1.9% of FA-mRNAs encode FA proteins in HDFs (Figure S3B; Table S5). Consistently, ribosome profiling of FA isolates revealed that enriched mRNAs have a lower translation efficiency compared to non-enriched mRNAs (Figures S3C–S3E; Table S6; Data S1). However, *TLN1* and *FLNA* mRNAs, which encode FA proteins, showed full ribosome coverage. Together, these data suggest that FA-mRNAs not encoding FA proteins have a low translation rate (Figure S3F). G3BP1 binds to multiple elements within RNAs rather than a distinct consensus motif.[47,48] This is consistent with the apparent lack of consensus motifs in FA-mRNAs identified in our study (see STAR Methods). Overall, these findings suggest that FA-mRNAs share characteristics with SG mRNAs.

To further explore this point, we performed an *in vitro* RNP reconstitution assay to determine whether G3BP1 can form RNPs with FA-mRNAs (Figure 3A). We used protein and RNA concentrations comparable to those in SGs *in vitro*[25,49,50] and found that G3BP1 forms RNP complexes with *TRAK2*, *KIF1C*, *IMPAD1*, and *DCBLD2* FA-mRNAs (Figure 3A). These mRNAs were selected as proof-of-principle FA-mRNAs based on their length, levels at FAs, and low ribosome coverage (Figures S3F–S3H).

We next analyzed G3BP1 RNPs *in cellulo*. We found that endogenous G3BP1, but not iRFP, formed complexes at FAs in HDFs, and these complexes were disrupted by a 10-min RNase A treatment, supporting their classification as RNPs (Figure S3I). To investigate whether G3BP1 RNPs co-localize with FA-mRNAs, we detected endogenous *TRAK2*, *KIF1C*, *IMPAD1*, and *DCBLD2* (Figure 3B). Notably, G3BP1 RNPs co-localized with each of these FA-mRNAs at FAs, with a Pearson correlation coefficient of r = 0.865–0.945 for all comparisons ($p < 0.0001$), in approximately 90% of FAs where FA-mRNAs were localized (Figure 3C; Figure S3J). These findings suggest that G3BP1 and FA-mRNAs are present in RNP complexes at FAs.

Our data above indicate that G3BP1 binds FA proteins in an RNA-dependent manner. To test if FA-mRNA enrichment at FAs depends on G3BP1, we performed MERFISH of FA-mRNAs in HDFs with or without G3BP1, which was depleted using small hairpin RNA (shRNA) (Figure 3D; Figure S4A). Upon G3BP1 depletion, we observed a decreased FA spatial enrichment for 98% of the tested FA-mRNAs, with an average reduction of 1.5-fold ($p < 0.0001$), whereas their overall cellular abundance remained unchanged (Figures 3E and 3F; Figure S4B). This remains consistent even when accounting for differences in FA size between HDFs in treated and control conditions (Figure S4C). Furthermore, the depletion of G3BP1, but not G3BP2, substantially reduced *TRAK2* mRNA spatial enrichment at PXN-positive FAs (Figures S4E–S4H). Similarly, acute removal of G3BP1 by an auxin-inducible degron[51] significantly reduced (1.8-fold) the FA enrichment of *TRAK2* within 4 h (Figures S4F–S4J; Video S1), supporting the specificity of the shRNA approach.

Overall, our data suggest that G3BP1 and FA-mRNAs form RNP complexes at FAs in non-stressed cells.

G3BP1 RNP complexes regulate cell migration in unstressed cells

We investigated the role of G3BP1 in regulating the migration speed of individual HDFs. Notably, both continuous G3BP1 knockdown via shRNA over 24 h or acute G3BP1 degradation over 4 h using the auxin-inducible degron system decreased the mean migration speed of individual HDFs compared to controls (Figures S5A–S5D). As G3BP1 and G3BP2 are redundant in RNP formation,[25] we assessed each protein's contribution to cell migration. Depletion of G3BP2 impaired cell speed but not to the extent observed upon G3BP1 loss, and the combined loss of G3BP1 and G3BP2 showed no significant difference compared to the loss of G3BP1 alone (Figure S5E). Given G3BP1's role in promoting FA-mRNA spatial enrichment to FAs and the potentially redundant role of G3BPs in regulating cell migration, we focused our analysis on the effects of G3BP1 alone.

The NTF2-like (NTF2L) domain and RBD in G3BP1 (Figure 4A) are both required for SG formation in cells and liquid-liquid phase separation *in vitro*.[25] These domains support G3BP1 dimerization and RNA binding, respectively.[25] Notably, cell migration in G3BP1 shRNA-treated HDFs was restored to control levels with the re-expression of the full-length G3BP1 protein but not with G3BP1ΔNTF2L or G3BP1ΔRBD (Figures 4B and 4C; Videos S2, S3, S4, S5, and S6). Consistent with its role in FA function, full-length G3BP1 localized at FAs in G3BP1 shRNA HDFs, whereas the deletion mutants G3BP1ΔNTF2L

and G3BP1ΔRBD failed to restore localization to control levels (Figures 4D and 4E). These findings suggest that G3BP1 RNPs form at FAs and are required for cell migration.

To test if heterologous G3BP1 RNPs can regulate cell migration at FAs, we employed the MS2 coat protein (MCP) and MS2 binding site system[52] (see STAR Methods; Figure 4F). To ectopically recruit *TRAK2* mRNA to FAs, we fused 24 MS2 stem loops to *TRAK2* mRNA and co-expressed it with an MCP-PXN fusion protein (Figures 4F–4H). Others have shown that local over-expression of endogenous MS2-tagged *ACTB* mRNA increases FA size,[10] and a similar effect can be replicated by us with an ectopic MS2-*ACTB* strategy (Figure S5F). G3BP1 localization to FAs and migration speed increased in cells co-expressing MCP-PXN with ectopic MS2-*TRAK2* mRNA but not MS2 RNA controls (Figures 4I–4K; Figure S5G; Videos S7 and S8). Importantly, the enhanced migration observed in the presence of MS2-*TRAK2* mRNA was abolished in cells lacking G3BP1 (Figures 4J and 4K; Videos S9 and S10).

Overall, these data suggest that G3BP1 RNPs at FAs regulate cell migration.

G3BP1 regulates cell migration concurrently with protein synthesis inhibition

Our data suggest that G3BP1-FA-mRNA complexes regulate cell migration. Given that G3BP1 has been shown to regulate translation in other cells in both stress and non-stress conditions,[53–55] we examined whether it functions in cell migration by regulating translation. First, we conducted a protein puromycinylation assay by incubating whole cells or FA isolates from HDFs with puromycin for 5 min, followed by the analysis of the nascent proteomes using western blotting. Importantly, we observed no global differences in nascent proteins in whole cells or FA isolates from cells with or without G3BP1 (Figures 5A and 5B; Figures S6A and S6B). Consistently, the loss of G3BP1 did not alter the levels of core FA proteins, such as PXN, or FA-mRNA-encoded proteins like TRAK2, TALIN1, and ACTB (Figure 5C). These results suggest that protein synthesis is not reduced with the loss of G3BP1.

As an alternative approach, we treated HDFs with 100 μg/mL of cycloheximide (CHX) in the presence or absence of G3BP1. CHX used at 100 μg/mL interferes with the translocation step in protein synthesis and has been shown to inhibit FA function in mouse embryonic fibroblasts by blocking *ACTB* translation at FAs.[10] As expected, CHX treatment reduced HDF migration in shRNA controls (Figures 5D and 5E; Videos S11 and S13). However, G3BP1 loss further decreased the migration speed of CHX-treated HDFs (Figures 5D and 5E; Videos S12 and S14), suggesting that G3BP1's role in regulating migration can occur concurrently with altered protein synthesis. Consistently, *ACTB* mRNA and ZBP1/IGF2BP1 remain localized at FAs upon G3BP1 depletion (Figures S6C and S6D). Additionally, both G3BP1 and G3BP2 remain enriched at FA isolates during CHX treatment (Figure S6E). Finally, both MS2-TRAK2 mRNA, which is translated and produces protein, and MS2-TRAK2 mRNA lacking the initiating ATG codon, which does not result in protein production, increase migration speed in the presence of PXN-MCP (Figures 4F–4K; Figures S6F–S6K). These effects were only observed when G3BP1 was present, suggesting that FA-mRNA protein production may not be required for G3BP1 RNP function (Figures S6J and S6K).

These findings suggest that neither FA protein synthesis nor FA-mRNA translation is altered with the loss of G3BP1.

G3BP1 RNP complexes regulate FA protein mobility

Cell speed is a complex mechanism driven by FAs and strongly correlates with the average size of FAs rather than their number, shape, or surface density.[56] Hence, we measured the size of PXN-positive adhesions in HDFs lacking G3BP1. Consistent with the decreased migration speed, we found that G3BP1-deficient HDFs—depleted either via shRNA or the degron system—exhibited smaller PXN-positive adhesions (Figures 6A and 6B; Figures S7A and S7B). Importantly, G3BP1's effect on FA size persisted even when translational elongation was inhibited with CHX, suggesting that the reduction in PXN-positive adhesion size was independent of cytosolic or PXN protein synthesis (Figures 6A and 6B).

Besides protein abundance, the size of FA complexes is influenced by the dynamic exchange of FA proteins between the cytoplasm and FAs.[7] Thus, we investigated whether G3BP1 regulates PXN-positive adhesion size by altering PXN protein mobility using fluorescence recovery after photobleaching (FRAP).[6,7] PXN mobility was analyzed in both the presence and absence of G3BP1 under conditions of normal and halted protein synthesis. Notably, in cells lacking G3BP1, PXN exhibited a 31% reduction in FRAP, indicating a decrease in its mobile fraction (Figures 6C and 6D; Videos S15 and S16). In contrast, CHX treatment in HDFs did not affect PXN protein mobility (Figures 6C and 6D; Videos S17 and S18). Furthermore, FRAP of iRFP in the cytoplasm was unaffected by G3BP1 deficiency in HDFs (Figures S7C and S7D), suggesting that G3BP1 specifically regulates the mobility of FA proteins like PXN. Notably, re-expressing full-length G3BP1 in G3BP1-knockdown cells restored both PXN protein mobility and PXN adhesion size to control levels, whereas the G3BP1ΔRBP and G3BP1ΔNFTL2 mutants failed to do so (Figures 6E–6H; Videos S19, S20, and S21). These findings mirror the observed effects on cell migration.

Therefore, we propose that G3BP1 RNPs are required for maintaining the mobility of FA proteins, which in turn influences FA size and regulates cell migration (Figure 7).

DISCUSSION

Our work identified a role for G3BP1 RNPs in regulating FA function and cell migration in non-stressed cells. We discovered that a subset of cytoplasmic mRNAs, characterized by features typical of SG mRNAs such as longer coding regions and UTRs, low translation, and AU-rich elements, localizes to FAs along with SG proteins, including the key SG nucleating RBP, G3BP1. G3BP1 binds to and localizes with FA proteins in an RNA-dependent manner. In the absence of G3BP1, FA-mRNAs show reduced localization to FAs, and cell migration is impaired. Migration driven by the recruitment of exogenous FA-mRNA also requires G3BP1, underscoring its role in FA function as part of an RNP complex. Mechanistically, the RNA-binding and dimerization domains of G3BP1 are essential for promoting cell speed via increasing the size of FAs. In summary, our model suggests that G3BP1 RNPs regulate the dynamics of FA proteins, which in turn affects FA size and cell migration (Figure 7).

The FA-dependent G3BP1 interactome that we discovered in this study is enriched in many SG proteins,[42] including G3BP2 and several key proteins involved in translation regulation,[57] RNA metabolism (e.g., LARP1[58] and CSDE1[59]), and mRNA stability (IGF2BPs[60]). However, FAs do not contain other canonical SG nucleating proteins (e.g., UPF1, ATXN2, TIA1, and TIAR[25,61]). Moreover, RNA-dependent enrichment of G3BP1 at FAs was not affected by treatment with the translational inhibitor CHX, which prevents SG formation by stabilizing mRNAs on polysomes.[55] Furthermore, although FA-mRNAs share characteristics with SG-mRNAs, such as reduced translation at FAs, they differ in that FA-mRNAs are actively translated in HDFs, and their proteins are essential for normal cell functions. Thus, unlike SG mRNAs, FA-mRNA translation is not globally halted. However, the role of FA-mRNAs in G3BP1 RNPs can be compatible with their function as protein synthesis molecules (see limitations of the study). Overall, despite similarities with SGs, future studies are needed to understand how FA-mRNA-G3BP1 RNPs form a distinct type of local assembly in non-stressed cells.

How FA-mRNAs are recruited to FAs and G3BP1 RNPs is unknown. Analysis of FA-mRNA sequences did not reveal any consensus sequences. For example, FA-mRNAs do not contain the sequence motif that binds to ZBP1/IGF2BP1, the RBP responsible for mediating the transport and local translation of β-actin mRNA.[62] Consistently, the loss of G3BP1 did not disturb the β-actin mRNA and ZBP1/IGF2BP1 localization. We note that some FA-mRNAs, such as *TRAK2* and *NET1*, have pyrimidine-rich motifs in their 5′ UTRs, which can recruit the RBP LARP1,[63] a G3BP1 binding partner. Hence, some FA-mRNAs may recruit LARP1, or vice versa, via these motifs. Furthermore, intermolecular RNA-RNA contacts could guide the self-assembly of RNPs at high RNA local concentrations.[64] G3BP1 also exhibits "condensate chaperone" functions, promoting intermolecular RNA-RNA interactions to stabilize RNA condensates *in vitro* and *in vivo*.[50] G3BP1 RNPs could also form at lower local RNA concentrations,[65] particularly if they rely on the self-assembly of highly interacting proteins, such as FA proteins and G3BP1-FA proteins. In support of this model, FA proteins are known to phase separate to promote integrin clustering.[66] This would also explain why G3BP1 loses its protein interaction network in the absence of either FAs or RNA.

Cell migration of individual adherent cells is a complex mechanism that relies on the continuous reorganization of FAs and the cytoskeleton.[2] This reorganization of FAs includes formation, maturation, and disassembly; each stage requires FA proteins to move in and out of the adhesion.[6–8,67] Here, we propose that G3BP1 RNPs promote the mobility of an FA protein within the adhesion complex by directly interacting with a variety of FA proteins (such as TLN1 and ACTN1). However, G3BP1 RNPs could also regulate the mobility of FA proteins that directly bind to G3BP1 and indirectly influence the dynamics of FA proteins within the adhesion. For instance, the decreased PXN protein mobility, detected upon G3BP1 loss, may result from altered interactions of PXN with other FA proteins that directly bind to G3BP1 or overall changes in mechanical forces on the adhesion.[6,68–70] Further work will be needed to elucidate what domain(s) of G3BP1 directly binds to FA proteins, how RNA facilitates these interactions, and the dynamics of multiple FA proteins that bind indirectly to G3BP1. Growing evidence exists for a relationship between FAs, RNPs, and phase separation behaviors. For instance, the FA protein p130Cas forms

phase-separated-like structures containing mRNAs, which bud from FAs in high-adhesion conditions.[71] p130Cas and FA kinase undergo liquid-liquid phase separation *in vitro*, which may promote integrin clustering.[66] PXN has also been shown to undergo phase separation, which nucleates FA components and accelerates cell spreading.[72] Hence, the liquid-liquid phase separation behavior of FA proteins and G3BP1 might help explain the direct or indirect change in FA protein mobility in the absence of G3BP1.

Here, we suggest that G3BP1 RNPs impact the dynamics of FA proteins, thereby influencing the overall function of the macromolecular protein complex in living cells. How RNPs can modulate protein mobility remains a subject for continued exploration in the field. Previous research shows that non-coding or untranslated RNA sequences in multimerized states can function as crowding agents. For example, nuclear droplets of nascent or long non-coding RNAs contain elements that can pull together even very distal regions of the genome to regulate transcriptional protein complexes.[73–75] Hence RNPs, like the one formed by G3BP1, can promote biochemical reactions directly by binding proteins within the RNP or indirectly by regulating the diffusion and increasing the local concentration of reaction components, such as other nucleic acid molecules and proteins.

Cell migration is a key response to the mechanotransduction of the extracellular matrix and is essential for biological processes like wound healing, invasion, or signaling. In a sense, FAs are sentinels of “environmental change.” Thus, similar to SG RNPs, FA RNPs may enable cells to respond rapidly and appropriately to environmental fluctuations. When a cell loses its ability to sense mechanical environments, it triggers pathophysiological conditions, such as halted embryonic development, chronic wounds, or cancer metastasis.[76–78] The discovery that G3BP1 RNPs alter FA function potentially opens new avenues to manipulate aberrant matrix-cell interactions.

Limitations of the study

The role of G3BP1 in FAs was evaluated by globally removing G3BP1 in fibroblasts. To specifically manipulate G3BP1 at FAs, we considered generating a G3BP1 tagged with an auxin-inducible degradation system targeted to FAs by fusing mAID (auxin-inducible degron) to an FA-localized protein. Upon addition of IAA (auxin), the entire ubiquitin complex, which includes E2, RBX1, CUL1, SKP1, and exogenously expressed OsTIR1, is recruited to the tagged protein for degradation. While this method could enable the localized degradation of G3BP1 at FAs, the complexity and molecular weight of the degradation protein system could introduce unintended effects on FA protein function, potentially leading to confounding results. Further tools will need to be developed to directly test the effect of G3BP1 at FAs. However, we observed effects on cell migration following the removal of G3BP1 for 4 h, which were consistent with the sustained protein depletion observed using shRNA. Since cell migration is a rapid process dependent on FA function, these findings support an FA-specific role for G3BP1. Furthermore, heterologous G3BP1 RNPs at FAs, as well as the re-expression of full-length G3BP1 that restores its localization to FAs in G3BP1-depleted cells, regulate cell migration, supporting the proposed function of G3BP1 at FAs.

We examined FA-mRNA function in G3BP1-dependent cell migration using TRAK2 tagged with MS2 co-expressed with MCP-PXN. In our system, we used MS2 tagging of an exogenous mRNA to FA, which is an artificial approach to form G3BP1 RNP complexes. However, tagging ACTB-MS2 produced similar effects on FA size, as previously reported using endogenous ACTB tagging, indicating that exogenous expression can recapitulate endogenous tagging. Future work is needed to explore the effects of FA-mRNA-G3BP1 RNPs in an endogenous context.

Since FA-mRNAs are inefficiently translated at FAs and their proteins are, for the most part, not found at FAs, we suggest that the mRNA protein synthesis at FAs is not the primary reason behind their local enrichment. However, the role of mRNAs at FAs can be compatible with their function as protein synthesis molecules, as most mRNAs cycle between an active and inactive translational “burst” where, during the inactive phase, mRNA could be entangled with G3BP1 RNPs.

We acknowledge that visualizing the formation and dynamics of G3BP1-FA-mRNAs and FA protein complexes will require further mechanistic studies requiring higher-resolution microscopy in living cells. FAs are highly dynamic complexes that assemble and disassemble within minutes. Consequently, G3BP1 and FA-mRNAs may form transient RNPs at FAs, depending on the state of the adhesions. In this study, we were able to visualize G3BP1 and FA-mRNA RNP complexes only in fixed cells and using standard confocal microscopy with an Airyscan module, which increases the resolution in all three dimensions (140 nm in x and y and 400 nm in z) but requires linear deconvolution. We have rigorously tested multiple negative controls to confirm the presence of G3BP1 RNP complexes at FAs, including RNase treatment, G3BP1 shRNA, and reconstitution with G3BP1 mutants lacking the RNA-binding or dimerization domain, all of which support the existence of localized G3BP1 RNPs at formed FAs.

RESOURCE AVAILABILITY

Lead contact

Requests for further information and resources should be directed to and will be fulfilled by the lead contact, Stefania Nicoli (stefania.nicoli@yale.edu).

Materials availability

Plasmids generated in this study are available upon request.

Data and code availability

- All RNA sequencing data generated in this study were deposited at GEO under SuperSeries GEO: GSE246956 or can be found individually at GEO: GSE246955 and GSE246499 and are available as of the date of publication. All proteomics data generated in this study were deposited at PRIDE: PXD059392 and are publicly available as of the date of publication.
- Open-source codes for MERFISH imaging are available at https://github.com/ZhuangLab/storm-control.

- All data reported in this paper will be shared by the lead contact upon request.
- Any additional information required to reanalyze the data reported in this paper is available from the lead contact upon request.

STAR★METHODS

EXPERIMENTAL MODEL AND STUDY PARTICIPANT DETAILS

All cells were cultured at 37°C, 5% CO_2, and 95% relative humidity. Human umbilical vein endothelial cells (HUVECs) were purchased from Cell Applications Inc. (200–05n) from a Caucasian male (Lot #: 3118). Cells were screened by manufacturer for bacteria, yeast, fungi, mycoplasma, virus and authenticated for positive VERGF2 pathway activation following stimulation by VEGF. HUVECs were cultured on dishes coated with 0.1% w/v gelatin (10 min at room temperature in PBS; Sigma) in M199 medium (11150-059, ThermoFisher) supplemented with 20% FBS (F0926-500 ML, Sigma), supplemented with 10 μg/mL endothelial cell growth supplement prepared from bovine hypothalamus, 50 μg/mL heparin filtered (H3149-100KU, Sigma), and 1% Penicillin-Streptomycin (15140122, ThermoFisher). Cells were cultured according to manufacturer's instructions and used until passage 6. Human dermal fibroblasts (HDFs) were purchased from the American Type Culture Collection (ATCC, PCS-201-010, Lot: #80825173) derived from the foreskin of a neonate, Middle Eastern male. Cells were screened by manufacturer for bacteria, yeast, fungi, mycoplasma, virus and authenticated using positive TE-7, a fibroblast marker, and negative Pan-Cytokeratin, an epithelial marker, expression. HDFs were cultured in fibroblast growth medium (ATCC, PCS-201-030) supplemented with the Fibroblast Growth Kit-Low Serum (ATCC, PCS-201-041), 0.5 mL Phenol Red (ATCC, PCS-999-001, final concentration 33 μM) and 1% Penicillin-Streptomycin (ThermoFisher, 15140122). HDFs were cultured according to manufacturer's recommendations and used until passage 6. For generation of lentivirus, Lenti-X 293T cells were used (Takara, 632180) and tested for mycoplasma. Cells were cultured in DMEM, high glucose, GlutaMAX (Gibco, 11995) supplemented with 10% FBS (F0926-500 ML, Sigma), and 1% Penicillin-Streptomycin (15140122, ThermoFisher).

METHOD DETAILS

Focal adhesion isolation—Focal adhesions were isolated as previously described.[26] Cells were seeded on tissue culture plastic coated with bovine plasma fibronectin (10 μg/mL in PBS overnight at 4°C). After 24 h in culture, cells were rinsed once with PBS and then treated for 3 min in a 2.5 mM triethanolamine (Sigma, 90279–100ML) low ionic strength buffer, pH 7.0. Immediately after the incubation, cell bodies were removed using hydrodynamic force (setting 1, Interplak, Conair) using PBS at ~0.5 cm from and ~90° to the surface of the dish. Dishes were immediately inspected for removal of cell bodies using phase microscopy. Isolated FAs were washed 3 times with PBS before fixation or collection from the dish using a cell scraper (LabScientific, CL-25) in the required buffer for further analysis.

mRNA- and ribo-seq library preparation—Total RNA was extracted from four replicates of isolated FA samples (each replicate was pooled from four 100 mm dishes)

or matched whole cell controls from HUVECs or HDFs using TRIzol reagent (Invitrogen, 15596026) according to the manufacturer's protocol. Prior to mRNA-seq library preparation, RNA was run on a 2100 Bioanalyzer (Agilent Technologies, Inc.) to ensure high quality RNA. Then, 500 ng of total RNA was used to prepare Lexogen QuantSeq 3′ mRNA-Seq FWD libraries for Illumina deep-sequencing according to the manufacturer's protocols. Libraries were amplified for 13–14 PCR cycles. Ribo-Seq samples were prepared according to manufacturer's instructions using the RiboLace Kit from Immagina BioTECHNOLOGY (RL001). For these samples, cells were treated for 5 min with 10 μg/mL cycloheximide (C4859–1ML, Sigma) at 37°C directly prior to focal adhesion isolation or collection of whole cell samples.

High-throughput sequencing analysis—For record keeping and configuring the bioinformatics analysis, samples annotations were stored in LabxDB.[80] Export to the Sequence Read Archive was achieved using the "export_sra.py" script from LabxDB-tools [https://github.com/vejnar/LabxDB-tools]. Annotations of human genes and the genome sequence of GRCh38 assembly was obtained from Ensembl 92[81]. The "import_ensembl" script from the FONtools[82] was used to (i) download FASTA and GFF3 files from Ensembl, (ii) create an index of the human genome, and (iii) generate FON1 files containing gene and transcript annotations.

QuantSeq RNA-seq and motif analysis—Raw reads were processed using LabxPipe (https://github.com/vejnar/LabxPipe): first reads were trimmed using ReadKnead (https://github.com/vejnar/ReadKnead) using the "bktrim" algorithm[83] using the sequence AAAAAAAAAAAAAAAGATCGGAAGAGCACACGTCTGAACTCCAGTCAC. They were then mapped to the human genome using STAR[84] with non-default parameters "–alignEndsType Local" and "–seedSearchStartLmaxOverLread 0.8". FON1 files containing genes (or "metagenes") were generated by concatenating the isoforms of each gene together using the "–method union" option of the "fon_transform" tool.[82] Read counts per gene were computed by summing the total number of reads overlapping at least 10 nucleotides of the gene (i.e., meta-gene) annotation. Reads mapping to multiple loci were accounted for by dividing 1 (each read) by the number of loci to which the read was mapped to. To identify differentially expressed genes, genes with at least 1 count in both conditions in any of the replicates were first selected, and input to the "DESeq" function.[84] The "results" function with parameters "pAdjustMethod = "fdr", independent-Filtering = FALSE" returned the differentially expressed genes. To identify enriched motifs in FA-mRNAs, HOMER Motif Discovery and Analysis was used on FA-mRNA sequences.[39] Comparing to a background size of 1x (119 or 236 non-enriched mRNAs expressed in HDFs and HUVECs, respectively), no motifs were identified. When expanding the background to 10x (1190 or 2360 non-enriched mRNAs expressed in HDFs and HUVECs, respectively) only 2–4 motifs with a *p*-value of 1e-6 were identified which is orders of magnitude below the typical *p*-value for biologically meaningful motif identification.

Ribo-seq analysis—Raw reads were first trimmed using ReadKnead (https://github.com/vejnar/ReadKnead) using the "bktrim" algorithm. Trimmed reads were then filtered of small RNAs by mapping them onto sequences extracted from RepeatMasker[85] (rRNA,

snRNA, scRNA and tRNA types) and Ensembl[81] (rRNA, snoRNA, snRNA, misc_RNA, Mt_rRNA and Mt_tRNA types) using STAR[84] with the non-default parameters "–alignEndsType Local", "–seedSearchStartLmaxOverLread 0.8" and "–outReadsUnmapped Fastx". Unmapped reads (obtained from the last option above) were then mapped to human genome using STAR with the non-default options "–alignEndsType EndToEnd" and "–seedSearchStartLmaxOverLread 0.8". The coding sequences (in genomic coordinates from FON1 file) were shifted of 12 nucleotides upstream to take into account the nucleotide separating the read start from the P-site of the translating ribosome. Read counts per mRNA were computed by summing the total number of reads overlapping at least 10 nucleotides the shifted mRNA annotation. Reads mapping to multiple loci (up to 5 loci) were accounted for by dividing 1 (each read) by the number of loci to which the read was mapped to. Ribosome profiling plots were obtained following Python notebook published at https://github.com/vejnar/notebooks/blob/main/ribosome_profiling/ribo_orf_plot.ipynb. Translational Efficiency was calculated as ribosome protected TPM divided by the mRNA TPM as performed previously.[31]

FA-mRNA properties—mRNA length was reported from the longest isoform of annotated protein-coding genes. 3′UTR length is the full-length 3′UTR length obtained from Refseq (hg19). For counting of AU-rich elements, we only considered the canonical sequence AUUUA. We counted the number of AU-rich elements in annotated 3′UTRs of mRNAs expressed in HDFs or HUVEC. All values are listed in Table S1.

RT-qPCR—For RT-qPCR, RNA was prepared as described above using TRIzol reagent (Invitrogen, 15596026) according to the manufacturer's protocol. 500 ng of RNA was converted to cDNA (SuperScript IV, ThermoFisher 18090010) and used as template for SYBR Green-based qPCR (Kapa Biosystems, KR0389). The double delta Ct analysis method was used to determine relative gene expression using *ACTB* as a housekeeping gene as it was expressed at equal amounts in both whole cell and isolated FAs, determined by mRNA-seq. All primers are listed in Table S1.

Probe design

MERFISH probe design: The template oligo pools of Focal Adhesion mRNA MERFISH (122 transcripts) and Control mRNA MERFISH (133 negative control transcripts +3 periphery associated transcripts) were designed similarly to that previously described,[32] for enzymatic amplification of the RNA MERFISH primary probes targeting the transcripts of focal adhesion genes and control genes, respectively. Briefly, each oligo in the template oligo pools contained six regions: 1) a 20-nt 5′ forward priming region, 2) a 20-nt readout region, 3) a 30-nt primary hybridization region, 4) a second 20-nt readout region, 5) a third 20-nt readout region, and 6) a 20-nt 3′ reverse priming region. The priming regions were selected according to a previous MERFISH study.[32]

The 16 readout sequences were selected from a previous publication.[86] Modified Hamming-Distance 4 (MHD4) coding scheme[32] was used for combinatorial barcoding. Each RNA species (gene) was represented by a unique set of 4 out of 16 readout sequences. Each oligo in the template oligo pools harbors 3 of the 4 selected readout sequences, which

shuffles among the oligos targeting the same gene. Each gene is targeted by 48 oligos. Therefore, each of the 4 selected readout regions appears 36 times on the 48 oligos for the corresponding target gene.

The primary hybridization regions were chosen from the focal adhesion-enriched genes via OligoArray 2.1 (for FA-mRNA MERFISH library)[87] or ProbeDealer (for control MERFISH library)[33] with the following criteria: 1) The melting temperature of the oligos is not lower than 66°C; 2) the oligos do not cross-hybridize with each other at 72°C or higher temperature; 3) the oligos cannot form stable secondary structures at 76°C or higher temperature; 4) there is no consecutive repeats of six or more identical bases in the sequence; and 5) the oligos do not overlap with each other. The qualified oligos were then screened against human transcriptome Ensembl 92 by BLAST+,[88] and oligos with significant homology with transcripts from more than one gene were excluded. 48 primary hybridization regions were selected for each target gene.

Single-molecule FISH probe design: The single-molecule FISH (smFISH) primary probes of the following genes were enzymatically amplified from a template oligo pool: *TLN1*, *CALD1*, *MACF1*, *CTNNB1*, *PPP1R12A*, *IQGAP1*. Each oligo contained four regions: 1) a 20-nt 5′ forward priming region, 2) a 30-nt readout region, 3) a 30-nt primary hybridization region, and 4) a 20-nt 3′ reverse priming region. The priming region sequences and the readout region sequence were chosen according to a previous study.[32] The primary hybridization regions were designed as introduced above. 36 primary hybridization regions were selected for each target gene.

The smFISH primary probes of *ACTB*, *SKP1*, *KPNA4*, *FLNB*, *TRAK2*, *KIF1C*, *DCBLD2*, *IMPAD1*, *ZMPSTE24*, and *STEAP3* were individually ordered from DNA Technology (IDT), Inc., which carried the following two regions: 1) a 30-nt primary hybridization region, and 2) a 30-nt readout region. The primary hybridization regions were designed as introduced above. 36–48 primary hybridization regions were selected for each target gene. The selected primary hybridization regions were then appended a 30-nt readout region selected from a previous study.[32]

Probe synthesis: Template oligo pools were ordered from CustomArray, GenScript. MERFISH primary probes and a subset of smFISH primary probes specified in the section above were then synthesized through an enzymatic amplification procedure reported in previous studies.[32,86] Briefly, oligo pools were amplified through limited-cycle PCR and *in vitro* transcription and converted to single-stranded DNA via reverse transcription, alkaline hydrolysis and column purification. Synthesized primary probes were dried by ThermoFisher SpeedVac DNA120 Vacuum Concentrator and stored at −20°C and resuspended in 10 μL ultrapure water before usage. Dye-labeled readout probes, the remaining smFISH primary probes specified in the section above, and PCR primers for probe synthesis were ordered from DNA Technology (IDT), Inc.

smFISH and FA spatial enrichment: HDFs were seeded on 25 mm coverslips in 6-well dishes coated with bovine plasma fibronectin (10 μg/mL in PBS overnight at 4°C) and allowed to adhere overnight. All samples were fixed with 4% paraformaldehyde (Electron

Microscopy Sciences) in PBS for 10 min at room temperature and permeabilized in 0.5% Triton X-100 for 10 min. For the IF counterstain, the incubation steps were all conducted at room temperature. Samples were first blocked in 0.3% BSA in DPBS with RNase inhibitor (1:1000, NEB M0314L) for 30 min, then stained with anti-PXN (1:500, Abcam, ab32084) or anti-G3BP1 (1:400, Santa Cruz, sc-365338) and secondary (1:1000, ThermoFisher, A32731 or A11031) antibodies in DPBS with RNase inhibitor (1:1000) for 1 h each, and finally post-fixed in 4% paraformaldehyde for 10 min before proceeding with the smFISH hybridization. Cells were incubated in pre-hybridization buffer (50% formamide, 2× saline sodium citrate (SSC)) for 5 min at room temperature before proceeding to overnight smFISH primary hybridization. Cells were incubated at 37°C for 16–24 h in a humid chamber in 25μL primary hybridization buffer (50% formamide, 2× SSC, 0.1% w/v yeast tRNA (Life Technologies, 15401011), 10% dextran sulfate (Sigma, D8906) and 1:100 diluted murine RNase inhibitor (NEB M0314L) containing 40nM primary probes per primary probe sequence.

After primary hybridization, cells were washed twice in 2× SSC with 0.1% v/v Tween 20 at 60°C for 15 min each, followed by one wash in 2× SSC with 0.1% v/v Tween 20 at room temperature for 15 min. Cells were then incubated in secondary hybridization buffer (20% v/v ethylene carbonate (Sigma-Aldrich, E26258) in 2× SSC, 3nM readout probe) at room temperature for 25–30 min, and then washed 3 times with wash buffer (20% v/v ethylene carbonate in 2× SSC) for 5 min each. Samples mounted with Prolong Diamond Antifade with DAPI (Thermo, P36971) and imaged on a Leica SP8 or Zeiss LSM980 Airyscan 2 confocal.

To quantify localization to FAs, the centroid of each mRNA foci was calculated using previously published Mathematica code.[89] The same code was used to extract the FA mask. Using these two inputs, the distance between each FA and mRNA centroid was calculated with in house Python code. This gives two values from each image: the number of FA-mRNA foci colocalized with FAs and the number of FA-mRNA foci in the rest of the cell. From these values, we calculated mRNA foci density, defined as the number of mRNA foci per cell compartment area.[30,31] To determine if an mRNA is FA compartment-enriched, we calculated FA enrichment defined as the ratio of mRNA foci density at FA and mRNA foci density in the rest of the cell.[30,31] We represent the data as the Log of FA enrichment where a value of 0 represents no enrichment, a negative value represents negative enrichment, and a positive value represents positive enrichment.

To quantify the organization of mRNA, G3BP1, and FA proteins, the plot profile function in ImageJ was used. A region of interest (ROI) was drawn across an mRNA co-localizing with an FA and the intensity of each mRNA/protein was quantified and normalized to the max value across the ROI.

MERFISH imaging: MERFISH primary probe hybridization was conducted in the same way as smFISH introduced above, except that 1) HDFs were seeded on 1.5# coverslips of 40-mm diameter (Bioptechs, 40–1313-03193) that were coated by fibronectin (10 μg/mL in PBS overnight at 4°C), and 2) during primary hybridization, 25uL primary hybridization buffer containing 4–8 mM of primary probe sets were applied. Prior to overnight imaging,

fiducial beads (Spherotech, FP-0245–2 or Invitrogen, F8803) diluted in 2× SSC were applied to the cells, which served as markers for drift correction purpose during sequential imaging.

Imaging of the 16-bit MHD4 MERFISH scheme was conducted by 8 rounds of automated sequential hybridization, imaging and signal removal, using a Bioptech's FCS2 flow chamber and a home-built fluidic system.[32] The secondary probes of MERFISH were labeled at 5′ end with either Alexa Fluor 647 or Alexa Fluor 750 dyes, and in each round of readout hybridization, two secondary probes with the two different dyes were applied simultaneously and imaged sequentially, allowing the 16-bit MHD4 codes to be readout in 8 rounds of readout hybridization.

For each round of readout hybridization, cells were first treated with hybridization buffer (20% v/v ethylene carbonate (Sigma-Aldrich, E26258) in 2× SSC containing 3nM each of the corresponding MERFISH readout probes with Alexa Fluor 647 and Alexa Fluor 750 labeling, respectively, and 1:2000 diluted murine RNase inhibitor). Cells were incubated with hybridization buffer for 20 min at room temperature, and then 2 mL of wash buffer (20% v/v ethylene carbonate in 2× SSC) was applied to remove excessive readout probes. 2mL oxygen-scavenging imaging buffer (50 mM Tris-HCl pH 8.0, 5% w/v glucose, 2 mM Trolox (Sigma-Aldrich, 238813), 0.5 mg/mL glucose oxidase (Sigma-Aldrich, G2133), 40 μg/mL catalase (Sigma-Aldrich, C30), 1:2000 diluted murine RNase inhibitor in 2× SSC) was then applied to the sample for imaging multiple fields of view. A layer of mineral oil (Sigma, 330779) was applied on top of the imaging buffer in a reservoir tube to prevent continuous oxidation.

During sequential imaging, a series of z stack images was taken under illumination with 750-nm, 647-nm, 560-nm, 488-nm and 405-nm lasers sequentially. The 750-nm and 647-nm lasers were used for MERFISH readout hybridization dye excitation, the 560-nm laser for Paxillin antibody staining excitation, the 488-nm laser for ACTN1 antibody staining excitation, and the 488-nm or 405-nm laser for fiducial bead excitation. Two sets of z stack imaging parameters were used in MERFISH experiments: 1) the step size of the z stack images was 200 nm, with a full depth of 3.8 μm on the z dimension (, Figures 1F–1I, 2G, S1E and S1F); 2) the step size was 500 nm with a full z dimension depth of 3.5 μm (Figures S1E and 2G). The exposure time at each height was 0.4 s. After imaging was finished for all fields of view in the current readout imaging round, the existing sequential FISH signal were removed by formamide wash (Figures 1F–1I, 2G, S1E and S1F) or photobleaching (Figures S1E and 2G). To perform formamide wash, 65% formamide in 2× SSC was slowly but continuously applied to the sample for 10 min and incubated with the sample for another 100 s. The excessive formamide was removed by washing the sample with 2× SSC buffer for 3 min. To perform photobleaching, 2× SSC buffer was applied to the sample, and then cells were exposed under 750-nm and 647-nm lasers for 29s.

After 8 rounds of sequential readout hybridization and imaging, 3mL of 1:1000 diluted DAPI (Thermo Scientific, 62248) in 2× SSC buffer was applied to the sample and let stand for 2 min. Imaging buffer was then applied to the sample, and z stack images for DAPI and fiducial beads were taken as described above.

MERFISH imaging system: A home-built microscope was used for MERFISH experiments, which consists of a Nikon Ti2-U body, a Nikon CFI Plan Apo Lambda 60× Oil (NA1.40) objective lens, and an active auto-focusing system.[90] A 750-nm laser (2RU-VFL-P-500–750-B1R, MPB Communications) was used to excite and image Alexa Fluor 750 on readout probes. A 647-nm laser (2RU-VFL-P-1000–647-B1R, MPB Communications) was used to excite and image Alexa Fluor 647 on readout probes. A 560-nm laser (2RU-VFL-P-1000–560-B1R, MPB Communications) was used to excite and image the secondary antibody for Paxillin staining. A 488-nm laser (2RU-VFL-P-500–488-B1R, MPB Communications) was used to excite and image the secondary antibody for ACTN1 staining and yellow-green fiducial beads. A 405-nm laser (OBIS 405 nm LX 50 mW, Coherent) was used to excite and image light yellow fiducial beads and the DAPI stain. A multi-band dichroic mirror (ZT405/488/561/647/752rpc-UF2, Chroma) was used on the excitation path to direct the five laser lines to the sample. A multi-band emission filter (ZET405/488/561/647–656/752 m, Chroma) and a Hamamatsu Orca Flash 4.0 V3 camera were installed on the emission path. The pixel size of the imaging system was 108 nm. An automated motorized x-y sample stage (SCAN IM 112 × 74, Marzhauser) was used to automatically image multiple fields of view.

MERFISH analysis

MERFISH decoding: MERFISH images were processed using MATLAB version R2022a using a previously reported pipeline.[91] Briefly, sample drift between sequential imaging rounds was corrected by fitting the fiducial beads markers with 2D Gaussian functions, identifying the movement of their center positions in x-y plane between the current imaging round and the first imaging round, and subtracting the movement by image translation. After drift correction, the full z stack was segmented at z dimension into smaller z-stacks that are 1 μm thick, and each was max projected along z dimension. The background of each image was derived by image opening using a disk-shaped structural element with an empirically determined radius of 5 pixels, and the background were subtracted from the raw RNA MERFISH image. The potential RNA signals were then identified by finding the regional maxima with pixels above a threshold, binarization, and dilation using a square structural element with a width of 3 pixels. To determine the optimal threshold for identifying RNA signals, an adaptive thresholding procedure was applied to each round of imaging, so that the relative abundance of identified RNA molecules in the imaging rounds fit the expected relative abundance derived from bulk RNA-seq data. This process was applied to all MERFISH readout imaging rounds for all fields of views. Afterward, at each z height, all 16-bits of binarized MERFISH readout images were assembled, and a 16-bit binary code was determined for each pixel. Pixels with a binary code that existed in the MERFISH codebook were recognized as RNA molecules. Adjacent pixels sharing the same code were processed as the same RNA molecule. For downstream analysis, the identified RNA molecules at each height were projected onto a single x-y plane along the z dimension.

Focal adhesion extraction: The Paxillin antibody staining in the 560-nm channel of the first imaging round was used to extract focal adhesions. The z stack of Paxillin antibody staining underwent mean projection along the z dimension and median filtering with MATLAB function medfilt2. The intensity of the filtered images was then re-scaled to between 0 and 1

by first subtracting the minimum intensity, and then divided by the maximum intensity after subtraction. The image background was derived by image opening using a diamond-shaped structural element with a size of 4 (strel('diamond',4)), and this background was then subtracted from the re-scaled image. The image further went through intensity adjustment using MATLAB function imadjust and image binarization. Focal adhesions were extracted from the binarized images by removing small objects from the binarized image that were smaller than 90 pixels. We noticed that high antibody staining background tended to appear in peri-nuclear region occasionally, which could be mis-identified as real focal adhesions, and therefore focal adhesion patterns within 15 pixels to the nucleus edge were removed.

Distance between focal adhesion and RNA: The RNA molecules were z-projected onto the x-y plane to calculate the 2D distance between RNAs and other cellular structures. The edges of binarized focal adhesions were extracted by Sobel methods, and the positions of the points on the edges were stored and further used in measuring distance between RNA and focal adhesion edge.

Focal adhesion enrichment analysis—For both MERFISH and smFISH, FA enrichment analysis was performed using mRNA localization and a PXN counterstain. FA enrichment is defined as the ratio of mRNA foci density at FA and mRNA foci density in the rest of the cell.[30,31] mRNA foci density is the number of mRNA per unit cell segment area. For direct colocalization, unit cell segment area was calculated based on PXN positive area (FA) vs. PXN negative area (rest of cell).

Simulation of random RNA localization—In house python code was used to simulate a random localization of mRNA within a cell. Existing cell and FA masks were used from biological samples after imaging and processing. FA masks were generated as described in FA size quantification[92] and cell masks defined the outline of the cell determined by maximizing fluorescent signal in the FA channel and taking the ROI in Fiji. To simulate random mRNA, random x,y coordinates were generated within the cell mask (which assumes a uniform cell thickness). For each simulated mRNA, the distance to the nearest FA, as defined by the FA mask, was measured. Simulations were run 500 times using 20 different cells and assuming a range of ~15–200 mRNA per cell similar to observed FA-mRNAs. FA enrichment was calculated as described above.

Mass spectrometry preparation and analysis—For proteomics analysis, total protein was extracted from isolated FA samples or matched whole cell controls from HDFs using TRIzol reagent (Invitrogen, 15596026) according to the manufacturer's protocol. Similarly, TRIzol was used on isolated FAs from control cells, cells treated with cycloheximide (100 μg/mL for 10 min) or cells treated with RNase A (1 mg/mL for 10 min) (four replicates for each group) before lysing. Protein and RNA were isolated to confirm the degradation of RNA in the RNase A treated samples. RNA was run on an agarose gel to determine RNA integrity and protein samples were air dried. For G3BP1 Co-IP samples, 3 100-mm plates of HDFs were pooled for each individual sample. Cells were treated with DMSO (equal volume to Blebb treated cells), RNase A (1 mg/mL for 10 min), or Blebb (25 mM for 30 min) prior to lysing in buffer with protease inhibitors (1:200, Millipore 539134) from the

MS compatible Co-IP kit (Thermo #90409) used according to manufacturers' instructions. Cell lysate was incubated with either an IgG Control (1:400, ThermoFisher, 31903) or G3BP1 antibody (1:40, Santa Cruz, sc-365338) for 24 h at 4°C and antigen-antibody complex was incubated with Protein A/G magnetic beads for 6 h at 4°C. After elution, samples were dried by ThermoFisher SpeedVac DNA120 Vacuum Concentrator. For all samples, the dried protein was sent to the Keck Mass Spectrometry & Proteomics Resource of the W.M. Keck Foundation Biotechnology Resource Laboratory at Yale University for liquid chromatography mass spectrometry analysis. Protein abundances were normalized to total abundances of detected spectral peaks for each sample.

Cell Immunostaining—For immunofluorescence analysis, FAs were fixed with 4% paraformaldehyde (Electron Microscopy Sciences) in PBS for 10 min. Cells were then washed and permeabilized in 0.5% Triton X-100 in DPBS with calcium and magnesium (Thermo, 21300025) for 5 min. Cells were blocked with 10% serum for 1 h, incubated for either 1 h at room temperature or overnight at 4°C with primary antibodies, and incubated for 1 h with secondary antibodies. Primary antibodies used were specific to VCL (1:500, Sigma, V9131), PXN (1:500, Abcam, ab32084), G3BP1 (1:400, Santa Cruz, sc-365338), ZBP1/IGF2BP1 (1:200, Millipore, HPA021367) or G3BP2 (1:400, Sigma, HPA018425). Secondary antibodies for either rabbit (1:1000, ThermoFisher, A-32731 or A-21244) or mouse (1:1000, ThermoFisher, A-11001 or A-21235) were applied. To stain F-actin, phalloidin (1:400, ThermoFisher, A12380) was added during the secondary antibody incubation step. Samples were mounted with DAPI in Fluoromount-G (Thermo, 00–4959-52) and imaged on a Leica SP8 confocal or Zeiss LSM980 Airyscan 2 confocal.

FA size and colocalization—To quantify FA size and colocalization with specific proteins, the following methods were applied using Fiji[79] (ImageJ) software.

To quantify FA size, Fiji[79] was used following a previously published method[92] and the steps are summarized here. (1) Background Subtraction: The background was subtracted using the Subtract Background function, with the sliding paraboloid option and a rolling ball radius set to 50 pixels to reduce background noise. (2) Contrast Enhancement: The CLAHE (Contrast Limited Adaptive Histogram Equalization) plugin was used to enhance local contrast, followed by applying the EXP function and adjusting Brightness & Contrast to further reduce background interference. (3) Thresholding: The processed image was thresholded to isolate FA structures. (4) Particle Analysis: The Analyze Particles command was employed to measure FA size, extracting quantitative data.

To evaluate colocalization between RBPs or iRFP and FAs, the JACop plugin[93] was used to determine Pearson Correlation Coefficient. (1) FA Masking: The FA channel was processed similarly to the FA size analysis, retaining only the FA regions. (2) JACoP Plugin for Pearson Correlation: Using the JACoP plugin, the masked FA channel was paired with the channel of the protein of interest (e.g., RNA-binding proteins or iRFP-labeled proteins). The plugin calculated the Pearson Correlation Coefficient, providing a quantitative measure of colocalization between the protein of interest and the FA marker.

Immunoprecipitation for western blotting—For co-immunoprecipitation cells were culture to 90% confluence in 100 mm dishes before lysis in 500 mL of specified lysis buffer with protease inhibitors (1:200, Millipore 539134) and RNase inhibitors (1:100, NEB M0314L). Samples were treated prior to lysis with DMSO (equal volume to Blebb treated cells), RNase A (1 mg/mL for 10 min), or Blebb (25 mM for 30 min). For IP, the Pierce Classic Magnetic IP/Co-IP Kit (Thermo, 88804) was used according to manufactures' instructions for immunoprecipitation assays. Cell lysate was incubated with antibodies for IgG Isotype Control (1:400, ThermoFisher, 31235), Paxillin (PXN, Invitrogen, PA5–34910), G3BP1 (1:40, Santa Cruz, sc-365338), ACTN1 (1:40, Santa Cruz, sc-17829), or TLN1 (1:60, Millipore Sigma, T3287) for 24 h at 4°C and antigen-antibody complex was incubated with Protein A/G magnetic beads for 2 h at 4°C. Samples were eluted using low pH elution buffer, neutralized, and used for western blot analysis.

Western blots—For western blot analysis, cells or FA isolates were collected in RIPA buffer (Thermo 89900) with protease inhibitors (1:200, Millipore 539134), or the otherwise stated buffer, and protein concentration was determined by BCA assay (Thermo, 23225). Samples were loaded onto 4–12% SDS–PAGE gels, transferred on a Immun-Blot PVDF membrane (Bio-Rad), and blocked with 5% BSA or 5% milk for 1 h. Blots were then incubated with primary antibodies overnight at 4°C. Primary antibodies used were specific to ACTN1 (1:500, Santa Cruz, sc-17829), VCL (1:5000, Sigma, V9131), PXN (1:8000, Abcam, ab32084), TLN1 (1:2500, Abcam, ab104913), GAPDH (1:8000, Cell Signaling, 2118), AKT1/2/3 (1:200, Santa Cruz, sc-81434), α-Tubulin (1:1000, Millipore, 05–829), β-actin (1:500, Santa Cruz, sc-130656), PDI (1:400, Santa Cruz, sc-74551), TOM20 (1:100, Santa Cruz, sc-17764), G3BP1 (1:500, Santa Cruz, sc-365338), G3BP2 (1:1000, Sigma, HPA018425), Puromycin (1:4000, Millipore, MABE343), TRAK2 (1:1000, Invitrogen, PA5–21858), KIF1C (1:400, Novus Bioologicals, NBP1–85978), LARP1 (1:500, Sigma, SAB4500689), PPFIBP1 (1:750, Sigma, HPA001924), IQGAP1 (1:2000, Abcam, ab86064), NET1 (1:1000, Abcam, ab113202), RAI14 (1:500, Sigma, HPA036949), or CTNNB1 (1:4000, Sigma, C2206). Then, membranes were washed and incubated with secondary antibody anti-rabbit-HRP or anti-mouse-HRP (1:8000, Cell Signaling, 7076 and 7074) for 1 h at room temperature. After washing, blots were developed with super signal west pico chemiluminescent substrate (Thermo, 34580) using an SYNGENE G-Box imager. To detect newly synthesized proteins, cells were treated with puromycin (ThermoFisher, A1113803, 5 μM) for 5 min prior to lysing or FA isolation. Total protein was detected using Ponceau S solution prior to blocking (Sigma, P7170) and was removed with two 5 min washes with 0.1 N NaOH followed by two washes with TBS-T. Quantification was performed using ImageJ and normalized to either GAPDH or total protein as detected by ponceau S staining.

G3BP1 *in vitro* LLPS assay—Liquid-liquid phase separation (LLPS) assay experiments were all conducted at room temperature using human GFP-G3BP1 protein (a gift from Roy Parker's lab). FA-mRNA were *in vitro* transcribed using the T7 MEGAscript kit (AM1334, ThermoFisher) according to the manufacturer's protocol. To fluorescently label the RNA during *in vitro* transcription (IVT), 0.2 μL of 2.5 mM Cyanine 3-UTP (Enzo Life Sciences, 42505) was added during the reaction in addition to the kit components. Template sequences for full-length FA-mRNA were designed and purchased using GeneArt Gene synthesis from

Invitrogen with a T7 promoter on the 5′ end of full-length mRNA sequences for IVT. The transcription reaction was incubated for 3 h or overnight at 37°C and RNA was purified using lithium chloride precipitation. RNAs were dissolved in Nuclease-free water and stored at −20°C. Prior to LLPS, RNA was run on a denaturing gel to determine its integrity and a nanodrop was used to determine the concentration of RNAs. All experiments were conducted with 50 nM RNA, 10 μM GFP-G3BP1. RNA was incubated at 70°C for 2 min to denature unspecific binding[94] prior to being mixed with GFP-G3BP1 in PCR tubes before being transferred to a chamber created by a coverslip, a glass slide, and a double-sided spacer (Sigma GBL654002). Samples were imaged using an SP8 Leica confocal with a 63x objective. All images were captured within 20–30 min after LLPS induction.

Live cell culture treatments—For blebbistatin treatment, cells were cultured in media supplemented blebbistatin for a final concentration of 25 μM (Sigma, B0560) for 30 min. The blebbistatin was diluted in DMSO, therefore control cells were treated for 30 min with media supplemented with an equal volume of DMSO (VWR, IC0219605525). At the end of 30 min, cells were fixed for analysis. For cycloheximide (CHX) cells were treated for either 10 min, 1 h, or 2 h at a concentration of 100 μg/mL in cell culture media depending on the experimental setup (Sigma, C4859–1ML). 10 min was used to time match the RNase A treatment, 1 h was used due to the duration of the FRAP imaging, and 2 h was used to match the cell migration experiments. CHX has been used routinely to inhibit protein synthesis in as little as 2 min.[95] CHX was also diluted in DMSO, and an equal volume was added to control samples. For RNase A treatments, cells were cultured in media supplemented with RNase A (ThermoFisher, EN0531) for a final concentration of 1 mg/mL for 10 min prior to either FA isolation, lysing, or fixation. For sodium arsenite treatment, cells were treated at 500 μM for 45 min (Millipore Sigma, 1062771000).

Plasmid construction and lentiviral use—Plasmids for protein expression in cells were built using Gibson Assembly Master Mix (NEB, E2611) and designed using NEBuilder. PXN and PXN-mCherry were cloned from pmCherry Paxillin (Addgene, #50526). iRFP was taken from XSB407_pHR-iRFP670 plasmid (a gift from Xiaolei Su Lab). MS2 Stem loops were cloned from pET263-pUC57 24xMS2V7 (Addgene, #140705).[96] MCP-GFP was cloned from pUbC-nls-ha-stdMCP-stdGFP (Addgene, #98916).[97] Template sequences for full-length RNA were designed and purchased using GeneArt Gene synthesis from Invitrogen except for *ACTB* (Addgene #102718). For G3BP1 re-expression, the ΔRBD and ΔNTF2L plasmids (a gift from Paul Taylor) were cloned into the lentiviral backbone and fused with an SNAP tag for visualization to match full length G3BP1 (Addgene, #119949).

All inserts were generated via PCR using Q5 High-Fidelity DNA Polymerase (M0491L, NEB). Fragments were inserted into a pHAGE-UbiC backbone between the ClaI and NotI cut sites. Following a 15-min Gibson Assembly reaction, plasmids were transformed into 5-alpha Competent *E. coli* (NEB, C2987I), grown overnight, and colonies were isolated and sequenced to confirm assembly. To create ATG mutants, Q5 Site-Directed Mutagenesis Kit from NEB (E0554S) was used to remove 20 nt total around the ATG site for each mRNA.

To generate all lentiviruses, transfer plasmids (3 μg) were mixed with packaging (psPAX2, 2.25 μg) and envelope (pMD2.G, 750 ng) plasmids, then mixed with Lipofectamine 2000 (ThermoFisher, 11668019) for 20 min before being added to Lenti-X 293T cells. Virus containing supernatant was collected at 42, 66, and 90 h post-transfection, filtered, and stored at −80°C. Cells were then infected with filtered virus in the presence of polybrene (8 μg/mL) and used for experiments. Cells infected with shRNAs were used 3–5 days post infection. shRNAs for G3BP1 targeting the CDS (SHCLNG-NM_005754 and TRCN0000008723), G3BP1 targeting the 3′UTR for re-expression experiments (SHCLNG-NM_005754 and TRCN0000008719), G3BP2 (SHCLNG-NM_012297 and TRCN0000047550), TRAK2 targeting the 3′UTR (SHCLNG-NM_015049 and TRCN0000151916) or control shRNAs (MISSION pLKO.1-puro Non-Mammalian shRNA Control Plasmid DNA, SHC002) were purchased from Millipore Sigma as part of their MISSION Lentiviral shRNA collection. For live imaging and migration assays cells were used 48 h post the last infection.

G3BP1 removal using the degron system—The auxin-inducible degron (AID2) version 2 system was used to remove G3BP1 rapidly from cells.[51] Plasmids were generated as described above. To make Lenti-osTIR1(F74G)-P2A-BFP, P2A-BFP was taken from pHR-pSFFV-dCas9-SunTag-P2A-BFP-WPRE (Addgene #122151) and osTIR1 was taken from pAAV-hSyn-osTIR1(F74G) (Addgene #140730) inserted into a lentiviral backbone. To make Lenti-G3BP1-eGFP-AID2, AID2 and G3BP1-eGFP were taken from pMK262-RAD21-AID2-mClover3 (Addgene #140538) and G3BP1-GFP-GFP (Addgene #119950), respectively and put in a lentiviral backbone.

Cells were first infected with a G3BP1 3′UTR targeting shRNA (SHCLNG-NM_005754 and TRCN0000008719, Millipore Sigma) and treated with puromycin for 7 days to remove all non-infected cells then subsequently infected with G3BP1-eGFP-AID2 and os-TIR1(F74G)-P2A-BFP. Cells were then seeded according to the assay (WB, IF, live imaging). To remove G3BP1, samples were treated with 5-Ph-IAA (IAA, 1 μM, R&D Systems, 7392/10) in cell culture media. For smFISH and western blots, samples were fixed or lysed at the end of 5 h treatment. For live cell imaging for individual cell migration or FA dynamics, live imaging started after 3 h of treatment and continued through 5 total hours of IAA treatment. To test the effectiveness of G3BP1 degradation, cells were imaged every 30 min on an SP8 Leica confocal for 5 h from the start of IAA treatment.

Cell migration assays—Cells used for cell migration assays were first infected with the necessary plasmids (ex. shRNAs, degron system, MCP-MS2 system). For individual cell migration, cells were reseeded onto fibronectin-coated glass bottom dishes (10 μg/mL in PBS overnight at 4°C) 24–72 h following the last infection. Before imaging, cells were labeled with CellTracker Orange CMTMR Dye (1:1000, ThermoFisher, C2927) for 30 min at 37°C. Cells were imaged on a Leica SP8 confocal at 37°C every 30 s for 2 h. Tracking analysis was performed using the TrackMate software in ImageJ.[98] Rose plots were generated using in house python code.

FRAP analysis—HDFs were transduced with lentiviruses expressing PXN-iRFP, PXN-mCherry, or iRFP. The TIRF microscope armed with a 405-nm FRAP laser at 100x objective

was used to quench interest fluorescence region on individual focal adhesion or cytoplasmic iRFP located on cell plasma membrane. The recovery images were then subsequently acquired at 200 msec intervals for 30 s duration. The assay was performed at a temperature setting of 37°C. Images were analyzed by ImageJ. The recovery percentage was determined by fitting a one-phase association model in GraphPad Prism (v9.4.1) software. As expected, photobleached FA proteins did not recover 100% of their original recovery intensity in all conditions.[68,99–101] All images were taken with the same brightness, contrast, and laser intensity.

QUANTIFICATION AND STATISTICAL ANALYSIS

All the statistical analysis was performed using Prism versions 9.2.0, 9.4.0, or 10.0.2. Figure legends indicate the exact number of measurements or samples, as well as the statistical tests used. two-way ANOVA with multiple comparisons was used to test mean differences among two or more groups at multiple time points or with overlayed treatments (FA size, collective cell migration). One-way ANOVA with multiple comparisons was used to compare differences between multiple groups and two-way unpaired t test was used to compare when there were only two experimental groups. To test for correlation, the Pearson correlation calculation was performed with a two-tailed p-value in Prism. To test for normality, D'Agostino & Pearson, Anderson-Darling, Shapiro-Wilk, and Kolmogorov-Smirnov were used. Exact p-values and replicates are provided in figures captions. For all graphs, significance is represented as not significant (n.s.) $p > 0.05$, *$p \leq 0.05$, **$p \leq 0.01$,***$p \leq 0.001$, ****$p \leq 0.0001$. Distributions are represented as boxplots displaying the median, upper Q3, lower Q1, min and max. Bar graphs are represented as Mean ± STD. All graphs display individual values. All images were blinded for quantification.

Supplementary Material

Refer to Web version on PubMed Central for supplementary material.

ACKNOWLEDGMENTS

We thank Drs. R. Parker, P. Taylor, A. Horwich, A. Dall'Agnese, V. Greco, L. Case, P. Willoughby, W. Mei, and *Life Science* editors for all their assistance necessary for this project. We thank Drs. R. Parker and P. Taylor for sharing the GFP-G3BP1 protein and the G3BP1 mutant plasmids, respectively. The experiments detailed in the manuscript were supported by 1R21HL165342 and AHA 957692 awarded to S.N., F32GM133176 awarded to L.C.B., and T32HL007950, DP2 GM137414, and R01 HG011245 awarded to S.W. M.H. was supported by the China Scholarship Council. We thank the MS & Proteomics Resource at Yale University for providing the necessary mass spectrometers and biotechnology tools (S10OD02365101A1, S10OD019967, and S10OD018034). The Yale Center for Genomic Health provided all RNA sequencing support, funded by 1S10OD030363–01A1.

REFERENCES

1. Franz CM, Jones GE, and Ridley AJ (2002). Cell migration in development and disease. Dev. Cell 2, 153–158. 10.1016/s1534-5807(02)00120-x. [PubMed: 11832241]
2. Parsons JT, Horwitz AR, and Schwartz MA (2010). Cell adhesion: integrating cytoskeletal dynamics and cellular tension. Nat. Rev. Mol. Cell Biol. 11, 633–643. 10.1038/nrm2957. [PubMed: 20729930]
3. Krause M, and Gautreau A (2014). Steering cell migration: lamellipodium dynamics and the regulation of directional persistence. Nat. Rev. Mol. Cell Biol. 15, 577–590. 10.1038/nrm3861. [PubMed: 25145849]

4. Geiger B, Spatz JP, and Bershadsky AD (2009). Environmental sensing through focal adhesions. Nat. Rev. Mol. Cell Biol. 10, 21–33. 10.1038/nrm2593. [PubMed: 19197329]
5. Kanchanawong P, Shtengel G, Pasapera AM, Ramko EB, Davidson MW, Hess HF, and Waterman CM (2010). Nanoscale architecture of integrin-based cell adhesions. Nature 468, 580–584. 10.1038/nature09621. [PubMed: 21107430]
6. Stutchbury B, Atherton P, Tsang R, Wang DY, and Ballestrem C (2017). Distinct focal adhesion protein modules control different aspects of mechanotransduction. J. Cell Sci. 130, 1612–1624. 10.1242/jcs.195362. [PubMed: 28302906]
7. Lele TP, Thodeti CK, Pendse J, and Ingber DE (2008). Investigating complexity of protein-protein interactions in focal adhesions. Biochem. Biophys. Res. Commun. 369, 929–934. 10.1016/j.bbrc.2008.02.137. [PubMed: 18331831]
8. Vicente-Manzanares M, and Horwitz AR (2011). Adhesion dynamics at a glance. J. Cell Sci. 124, 3923–3927. 10.1242/jcs.095653. [PubMed: 22194302]
9. Wehrle-Haller B (2012). Structure and function of focal adhesions. Curr. Opin. Cell Biol. 24, 116–124. 10.1016/j.ceb.2011.11.001. [PubMed: 22138388]
10. Katz ZB, Wells AL, Park HY, Wu B, Shenoy SM, and Singer RH (2012). beta-Actin mRNA compartmentalization enhances focal adhesion stability and directs cell migration. Genes Dev. 26, 1885–1890. 10.1101/gad.190413.112. [PubMed: 22948660]
11. Katz ZB, English BP, Lionnet T, Yoon YJ, Monnier N, Ovryn B, Bathe M, and Singer RH (2016). Mapping translation 'hot-spots' in live cells by tracking single molecules of mRNA and ribosomes. Elife 5, e10415. 10.7554/eLife.10415. [PubMed: 26760529]
12. Vedula P, Kurosaka S, MacTaggart B, Ni Q, Papoian G, Jiang Y, Dong DW, and Kashina A (2021). Different translation dynamics of beta- and gamma-actin regulates cell migration. Elife 10, e68712. 10.7554/eLife.68712. [PubMed: 34165080]
13. Mukherjee J, Hermesh O, Eliscovich C, Nalpas N, Franz-Wachtel M, Maček B, and Jansen RP (2019). beta-Actin mRNA interactome mapping by proximity biotinylation. Proc. Natl. Acad. Sci. USA 116, 12863–12872. 10.1073/pnas.1820737116. [PubMed: 31189591]
14. Song T, Zheng Y, Wang Y, Katz Z, Liu X, Chen S, Singer RH, and Gu W (2015). Specific interaction of KIF11 with ZBP1 regulates the transport of beta-actin mRNA and cell motility. J. Cell Sci. 128, 1001–1010. 10.1242/jcs.161679. [PubMed: 25588836]
15. Huttelmaier S, Zenklusen D, Lederer M, Dictenberg J, Lorenz M, Meng X, Bassell GJ, Condeelis J, and Singer RH (2005). Spatial regulation of beta-actin translation by Src-dependent phosphorylation of ZBP1. Nature 438, 512–515. 10.1038/nature04115. [PubMed: 16306994]
16. Wang T, Hamilla S, Cam M, Aranda-Espinoza H, and Mili S (2017). Extracellular matrix stiffness and cell contractility control RNA localization to promote cell migration. Nat. Commun. 8, 896. 10.1038/s41467-017-00884-y. [PubMed: 29026081]
17. Chrisafis G, Wang T, Moissoglu K, Gasparski AN, Ng Y, Weigert R, Lockett SJ, and Mili S (2020). Collective cancer cell invasion requires RNA accumulation at the invasive front. P Natl Acad Sci USA 117, 27423–27434. 10.1073/pnas.2010872117.
18. Costa G, Bradbury JJ, Tarannum N, and Herbert SP (2020). RAB13 mRNA compartmentalisation spatially orients tissue morphogenesis. EMBO J. 39, e106003. 10.15252/embj.2020106003. [PubMed: 32946121]
19. Norris ML, and Mendell JT (2023). Localization of Kif1c mRNA to cell protrusions dictates binding partner specificity of the encoded protein. Genes Dev. 37, 191–203. 10.1101/gad.350320.122. [PubMed: 36859340]
20. Mili S, Moissoglu K, and Macara IG (2008). Genome-wide screen reveals APC-associated RNAs enriched in cell protrusions. Nature 453, 115–119. 10.1038/nature06888. [PubMed: 18451862]
21. Mardakheh FK, Paul A, Kümper S, Sadok A, Paterson H, Mccarthy A, Yuan Y, and Marshall CJ (2015). Global Analysis of mRNA, Translation, and Protein Localization: Local Translation Is a Key Regulator of Cell Protrusions. Dev. Cell 35, 344–357. 10.1016/j.devcel.2015.10.005. [PubMed: 26555054]
22. Pichon X, Moissoglu K, Coleno E, Wang T, Imbert A, Robert MC, Peter M, Chouaib R, Walter T, Mueller F, et al. (2021). The kinesin KIF1C transports APC-dependent mRNAs to cell protrusions. RNA 27, 1528–1544. 10.1261/rna.078576.120. [PubMed: 34493599]

23. Moissoglu K, Stueland M, Gasparski AN, Wang T, Jenkins LM, Hastings ML, and Mili S (2020). RNA localization and co-translational interactions control RAB13 GTPase function and cell migration. EMBO J. 39, e104958. 10.15252/embj.2020104958. [PubMed: 32946136]
24. Gasparski AN, Moissoglu K, Pallikkuth S, Meydan S, Guydosh NR, and Mili S (2023). mRNA location and translation rate determine protein targeting to dual destinations. Mol. Cell 83, 2726–2738. 10.1016/j.molcel.2023.06.036. [PubMed: 37506697]
25. Yang P, Mathieu C, Kolaitis RM, Zhang P, Messing J, Yurtsever U, Yang Z, Wu J, Li Y, Pan Q, et al. (2020). G3BP1 Is a Tunable Switch that Triggers Phase Separation to Assemble Stress Granules. Cell 181, 325–345. 10.1016/j.cell.2020.03.046. [PubMed: 32302571]
26. Kuo JC, Han X, Yates JR 3rd, and Waterman CM (2012). Isolation of focal adhesion proteins for biochemical and proteomic analysis. Methods Mol. Biol. 757, 297–323. 10.1007/978-1-61779-166-6_19.
27. Kuang R, Wang Z, Xu Q, Liu S, and Zhang W (2015). Influence of mechanical stimulation on human dermal fibroblasts derived from different body sites. Int. J. Clin. Exp. Med. 8, 7641–7647. [PubMed: 26221311]
28. Byfield FJ, Reen RK, Shentu TP, Levitan I, and Gooch KJ (2009). Endothelial actin and cell stiffness is modulated by substrate stiffness in 2D and 3D. J. Biomech. 42, 1114–1119. 10.1016/j.jbiomech.2009.02.012. [PubMed: 19356760]
29. Moro A, Driscoll TP, Boraas LC, Armero W, Kasper DM, Baeyens N, Jouy C, Mallikarjun V, Swift J, Ahn SJ, et al. (2019). MicroRNA-dependent regulation of biomechanical genes establishes tissue stiffness homeostasis. Nat. Cell Biol. 21, 348–358. 10.1038/s41556-019-0272-y. [PubMed: 30742093]
30. Horste EL, Fansler MM, Cai T, Chen X, Mitschka S, Zhen G, Lee FCY, Ule J, and Mayr C (2023). Subcytoplasmic location of translation controls protein output. Mol. Cell 83, 4509–4523. 10.1016/j.molcel.2023.11.025. [PubMed: 38134885]
31. Moor AE, Golan M, Massasa EE, Lemze D, Weizman T, Shenhav R, Baydatch S, Mizrahi O, Winkler R, Golani O, et al. (2017). Global mRNA polarization regulates translation efficiency in the intestinal epithelium. Science 357, 1299–1303. 10.1126/science.aan2399. [PubMed: 28798045]
32. Chen KH, Boettiger AN, Moffitt JR, Wang S, and Zhuang X (2015). RNA imaging. Spatially resolved, highly multiplexed RNA profiling in single cells. Science 348, aaa6090. 10.1126/science.aaa6090. [PubMed: 25858977]
33. Hu M, Yang B, Cheng Y, Radda JSD, Chen Y, Liu M, and Wang S (2020). ProbeDealer is a convenient tool for designing probes for highly multiplexed fluorescence in situ hybridization. Sci. Rep. 10, 22031. 10.1038/s41598-020-76439-x. [PubMed: 33328483]
34. Fazal FM, Han S, Parker KR, Kaewsapsak P, Xu J, Boettiger AN, Chang HY, and Ting AY (2019). Atlas of Subcellular RNA Localization Revealed by APEX-Seq. Cell 178, 473–490. 10.1016/j.cell.2019.05.027. [PubMed: 31230715]
35. Gene Ontology Consortium; Aleksander SA, Balhoff J, Carbon S, Cherry JM, Drabkin HJ, Ebert D, Feuermann M, Gaudet P, and Harris NL (2023). The Gene Ontology knowledgebase in 2023. Genetics 224, iyad031. 10.1093/genetics/iyad031. [PubMed: 36866529]
36. Ashburner M, Ball CA, Blake JA, Botstein D, Butler H, Cherry JM, Davis AP, Dolinski K, Dwight SS, Eppig JT, et al. (2000). Gene ontology: tool for the unification of biology. The Gene Ontology Consortium. Nat. Genet. 25, 25–29. 10.1038/75556. [PubMed: 10802651]
37. Ma W, Zhen G, Xie W, and Mayr C (2021). In vivo reconstitution finds multivalent RNA-RNA interactions as drivers of mesh-like condensates. Elife 10, e64252. 10.7554/eLife.64252. [PubMed: 33650968]
38. Ma W, and Mayr C (2018). A Membraneless Organelle Associated with the Endoplasmic Reticulum Enables 3'UTR-Mediated Protein-Protein Interactions. Cell 175, 1492–1506. 10.1016/j.cell.2018.10.007. [PubMed: 30449617]
39. Heinz S, Benner C, Spann N, Bertolino E, Lin YC, Laslo P, Cheng JX, Murre C, Singh H, and Glass CK (2010). Simple combinations of lineage-determining transcription factors prime cis-regulatory elements required for macrophage and B cell identities. Mol. Cell 38, 576–589. 10.1016/j.molcel.2010.05.004. [PubMed: 20513432]

40. Buchan JR, and Parker R (2009). Eukaryotic stress granules: the ins and outs of translation. Mol. Cell 36, 932–941. 10.1016/j.molcel.2009.11.020. [PubMed: 20064460]
41. Matsuki H, Takahashi M, Higuchi M, Makokha GN, Oie M, and Fujii M (2013). Both G3BP1 and G3BP2 contribute to stress granule formation. Gene Cell. 18, 135–146. 10.1111/gtc.12023.
42. Jain S, Wheeler JR, Walters RW, Agrawal A, Barsic A, and Parker R (2016). ATPase-Modulated Stress Granules Contain a Diverse Proteome and Substructure. Cell 164, 487–498. 10.1016/j.cell.2015.12.038. [PubMed: 26777405]
43. Calderwood DA, Yan B, de Pereda JM, Alvarez BG, Fujioka Y, Liddington RC, and Ginsberg MH (2002). The phosphotyrosine binding-like domain of talin activates integrins. J. Biol. Chem. 277, 21749–21758. 10.1074/jbc.M111996200. [PubMed: 11932255]
44. Roca-Cusachs P, del Rio A, Puklin-Faucher E, Gauthier NC, Biais N, and Sheetz MP (2013). Integrin-dependent force transmission to the extracellular matrix by alpha-actinin triggers adhesion maturation. Proc. Natl. Acad. Sci. USA 110, E1361–E1370. 10.1073/pnas.1220723110. [PubMed: 23515331]
45. Khong A, Matheny T, Jain S, Mitchell SF, Wheeler JR, and Parker R (2017). The Stress Granule Transcriptome Reveals Principles of mRNA Accumulation in Stress Granules. Mol. Cell 68, 808–820. 10.1016/j.molcel.2017.10.015. [PubMed: 29129640]
46. Namkoong S, Ho A, Woo YM, Kwak H, and Lee JH (2018). Systematic Characterization of Stress-Induced RNA Granulation. Mol. Cell 70, 175–187. 10.1016/j.molcel.2018.02.025. [PubMed: 29576526]
47. Meyer C, Garzia A, Morozov P, Molina H, and Tuschl T (2020). The G3BP1-Family-USP10 Deubiquitinase Complex Rescues Ubiquitinated 40S Subunits of Ribosomes Stalled in Translation from Lysosomal Degradation. Mol. Cell 77, 1193–1205. 10.1016/j.molcel.2019.12.024. [PubMed: 31981475]
48. Fischer JW, Busa VF, Shao Y, and Leung AKL (2020). Structure-Mediated RNA Decay by UPF1 and G3BP1. Mol. Cell 78, 70–84. 10.1016/j.molcel.2020.01.021. [PubMed: 32017897]
49. Guillen-Boixet J, Kopach A, Holehouse AS, Wittmann S, Jahnel M, Schlüßler R, Kim K, Trussina IR, Wang J, Mateju D, and Poser I (2020). RNA-Induced Conformational Switching and Clustering of G3BP Drive Stress Granule Assembly by Condensation. Cell 181, 346–361. 10.1016/j.cell.2020.03.049. [PubMed: 32302572]
50. Dylan M, Parker DT, and Roy P (2024). G3BP1promotes intermolecular RNA-RNA interactions during RNA condensation. Mol. Cell 2765, 00917. 10.1016/j.molcel.2024.11.012.
51. Yesbolatova A, Saito Y, Kitamoto N, Makino-Itou H, Ajima R, Nakano R, Nakaoka H, Fukui K, Gamo K, Tominari Y, et al. (2020). The auxin-inducible degron 2 technology provides sharp degradation control in yeast, mammalian cells, and mice. Nat. Commun. 11, 5701. 10.1038/s41467-020-19532-z. [PubMed: 33177522]
52. Vera M, Tutucci E, and Singer RH (2019). Imaging Single mRNA Molecules in Mammalian Cells Using an Optimized MS2-MCP System. Methods Mol. Biol. 2038, 3–20. 10.1007/978-1-4939-9674-2_1. [PubMed: 31407274]
53. Sahoo PK, Lee SJ, Jaiswal PB, Alber S, Kar AN, Miller-Randolph S, Taylor EE, Smith T, Singh B, Ho TSY, et al. (2018). Axonal G3BP1 stress granule protein limits axonal mRNA translation and nerve regeneration. Nat. Commun. 9, 3358. 10.1038/s41467-018-05647-x. [PubMed: 30135423]
54. Smith J, and Bartel DP (2024). The G3BP Stress-Granule Proteins Reinforce the Translation Program of the Integrated Stress Response. Preprint at bioRxiv. 10.1101/2024.10.04.616305.
55. Mollet S, Cougot N, Wilczynska A, Dautry F, Kress M, Bertrand E, and Weil D (2008). Translationally repressed mRNA transiently cycles through stress granules during stress. Mol. Biol. Cell 19, 4469–4479. 10.1091/mbc.e08-05-0499. [PubMed: 18632980]
56. Kim DH, and Wirtz D (2012). Focal adhesion size uniquely predicts cell migration. Mol. Biol. Cell 23, 319a.
57. Ivanov P, Kedersha N, and Anderson P (2019). Stress Granules and Processing Bodies in Translational Control. Cold Spring Harbor Perspect. Biol. 11, a032813. 10.1101/cshperspect.a032813.

58. Lahr RM, Fonseca BD, Ciotti GE, Al-Ashtal HA, Jia JJ, Niklaus MR, Blagden SP, Alain T, and Berman AJ (2017). La-related protein 1 (LARP1) binds the mRNA cap, blocking eIF4F assembly on TOP mRNAs. Elife 6, e24146. 10.7554/eLife.24146. [PubMed: 28379136]
59. Cornelis S, Tinton SA, Schepens B, Bruynooghe Y, and Beyaert R (2005). UNR translation can be driven by an IRES element that is negatively regulated by polypyrimidine tract binding protein. Nucleic Acids Res. 33, 3095–3108. 10.1093/nar/gki611. [PubMed: 15928332]
60. Huang H, Weng H, Sun W, Qin X, Shi H, Wu H, Zhao BS, Mesquita A, Liu C, Yuan CL, et al. (2018). Recognition of RNA N(6)-methyladenosine by IGF2BP proteins enhances mRNA stability and translation. Nat. Cell Biol. 20, 285–295. 10.1038/s41556-018-0045-z. [PubMed: 29476152]
61. Anderson P, and Kedersha N (2008). Stress granules: the Tao of RNA triage. Trends Biochem. Sci. 33, 141–150. 10.1016/j.tibs.2007.12.003. [PubMed: 18291657]
62. Nicastro G, Candel AM, Uhl M, Oregioni A, Hollingworth D, Backofen R, Martin SR, and Ramos A (2017). Mechanism of beta-actin mRNA Recognition by ZBP1. Cell Rep. 18, 1187–1199. 10.1016/j.celrep.2016.12.091. [PubMed: 28147274]
63. Goering R, Arora A, Pockalny MC, and Taliaferro JM (2023). RNA localization mechanisms transcend cell morphology. Elife 12, e80040. 10.7554/eLife.80040. [PubMed: 36867563]
64. Van Treeck B, and Parker R (2018). Emerging Roles for Intermolecular RNA-RNA Interactions in RNP Assemblies. Cell 174, 791–802. 10.1016/j.cell.2018.07.023. [PubMed: 30096311]
65. Tauber D, Tauber G, Khong A, Van Treeck B, Pelletier J, and Parker R (2020). Modulation of RNA Condensation by the DEAD-Box Protein eIF4A. Cell 180, 411–426.e16. 10.1016/j.cell.2019.12.031. [PubMed: 31928844]
66. Case LB, De Pasquale M, Henry L, and Rosen MK (2022). Synergistic phase separation of two pathways promotes integrin clustering and nascent adhesion formation. Elife 11, e72588. 10.7554/eLife.72588. [PubMed: 35049497]
67. Romer LH, Birukov KG, and Garcia JGN (2006). Focal adhesions - Paradigm for a signaling nexus. Circ. Res. 98, 606–616. 10.1161/01.RES.0000207408.31270.db. [PubMed: 16543511]
68. Le Devedec SE, Geverts B, de Bont H, Yan K, Verbeek FJ, Houtsmuller AB, and van De Water B (2012). The residence time of focal adhesion kinase (FAK) and paxillin at focal adhesions in renal epithelial cells is determined by adhesion size, strength and life cycle status. J. Cell Sci. 125, 4498–4506. 10.1242/jcs.104273. [PubMed: 22767508]
69. Humphries JD, Wang P, Streuli C, Geiger B, Humphries MJ, and Ballestrem C (2007). Vinculin controls focal adhesion formation by direct interactions with talin and actin. J. Cell Biol. 179, 1043–1057. 10.1083/jcb.200703036. [PubMed: 18056416]
70. Feng Z, Mao Z, Yang Z, Liu X, and Nakamura F (2023). The force-dependent filamin A-G3BP1 interaction regulates phase-separated stress granule formation. J. Cell Sci. 136, jcs260684. 10.1242/jcs.260684. [PubMed: 36806943]
71. Kumar A, Tanaka K, and Schwartz MA (2024). Focal adhesion-derived liquid-liquid phase separations regulate mRNA translation. Preprint at bioRxiv. 10.1101/2023.11.22.568289.
72. Liang P, Wu Y, Zheng S, Zhang J, Yang S, Wang J, Ma S, Zhang M, Gu Z, Liu Q, et al. (2024). Paxillin phase separation promotes focal adhesion assembly and integrin signaling. J. Cell Biol. 223, e202209027. 10.1083/jcb.202209027. [PubMed: 38466167]
73. Sabari BR, Dall'Agnese A, and Young RA (2020). Biomolecular Condensates in the Nucleus. Trends Biochem. Sci. 45, 961–977. 10.1016/j.tibs.2020.06.007. [PubMed: 32684431]
74. Cho WK, Spille JH, Hecht M, Lee C, Li C, Grube V, and Cisse II (2018). Mediator and RNA polymerase II clusters associate in transcription-dependent condensates. Science 361, 412–415. 10.1126/science.aar4199. [PubMed: 29930094]
75. Fox AH, Nakagawa S, Hirose T, and Bond CS (2018). Paraspeckles: Where Long Noncoding RNA Meets Phase Separation. Trends Biochem. Sci. 43, 124–135. 10.1016/j.tibs.2017.12.001. [PubMed: 29289458]
76. van Zijl F, Krupitza G, and Mikulits W (2011). Initial steps of metastasis: cell invasion and endothelial transmigration. Mutat. Res. 728, 23–34. 10.1016/j.mrrev.2011.05.002. [PubMed: 21605699]

77. Phan THG, Paliogiannis P, Nasrallah GK, Giordo R, Eid AH, Fois AG, Zinellu A, Mangoni AA, and Pintus G (2021). Emerging cellular and molecular determinants of idiopathic pulmonary fibrosis. Cell. Mol. Life Sci. 78, 2031–2057. 10.1007/s00018-020-03693-7. [PubMed: 33201251]

78. Raghow R (1994). The role of extracellular matrix in postinflammatory wound healing and fibrosis. Faseb. J. 8, 823–831. 10.1096/fasebj.8.11.8070631. [PubMed: 8070631]

79. Schindelin J, Arganda-Carreras I, Frise E, Kaynig V, Longair M, Pietzsch T, Preibisch S, Rueden C, Saalfeld S, Schmid B, et al. (2012). Fiji: an open-source platform for biological-image analysis. Nat. Methods 9, 676–682. 10.1038/nmeth.2019. [PubMed: 22743772]

80. Vejnar CE, and Giraldez AJ (2020). LabxDB: versatile databases for genomic sequencing and lab management. Bioinformatics 36, 4530–4531. 10.1093/bioinformatics/btaa557. [PubMed: 32502232]

81. Aken BL, Achuthan P, Akanni W, Amode MR, Bernsdorff F, Bhai J, Billis K, Carvalho-Silva D, Cummins C, Clapham P, et al. (2017). Ensembl 2017. Nucleic Acids Res. 45, D635–D642. 10.1093/nar/gkw1104. [PubMed: 27899575]

82. Vejnar CE FONtools, https://github.com/vejnar/fontools..

83. Jiang H, Lei R, Ding SW, and Zhu S (2014). Skewer: a fast and accurate adapter trimmer for next-generation sequencing paired-end reads. BMC Bioinf. 15, 182. 10.1186/1471-2105-15-182.

84. Dobin A, Davis CA, Schlesinger F, Drenkow J, Zaleski C, Jha S, Batut P, Chaisson M, and Gingeras TR (2013). STAR: ultrafast universal RNA-seq aligner. Bioinformatics 29, 15–21. 10.1093/bioinformatics/bts635. [PubMed: 23104886]

85. Smit AF, Hubley R, and Green P (1996). RepeatMasker. https://www.repeatmasker.org/.

86. Moffitt JR, Hao J, Wang G, Chen KH, Babcock HP, and Zhuang X (2016). High-throughput single-cell gene-expression profiling with multiplexed error-robust fluorescence in situ hybridization. Proc. Natl. Acad. Sci. USA 113, 11046–11051. 10.1073/pnas.1612826113. [PubMed: 27625426]

87. Rouillard JM, Zuker M, and Gulari E (2003). OligoArray 2.0: design of oligonucleotide probes for DNA microarrays using a thermodynamic approach. Nucleic Acids Res. 31, 3057–3062. 10.1093/nar/gkg426. [PubMed: 12799432]

88. Camacho C, Coulouris G, Avagyan V, Ma N, Papadopoulos J, Bealer K, and Madden TL (2009). BLAST+: architecture and applications. BMC Bioinf. 10, 421. 10.1186/1471-2105-10-421.

89. Buskermolen ABC, Kurniawan NA, and Bouten CVC (2018). An automated quantitative analysis of cell, nucleus and focal adhesion morphology. PLoS One 13, e0195201. 10.1371/journal.pone.0195201. [PubMed: 29601604]

90. Wang S, Moffitt JR, Dempsey GT, Xie XS, and Zhuang X (2014). Characterization and development ofphotoactivatable fluorescent proteins for single-molecule-based superresolution imaging. Proc. Natl. Acad. Sci. USA 111, 8452–8457. 10.1073/pnas.1406593111. [PubMed: 24912163]

91. Liu M, Lu Y, Yang B, Chen Y, Radda JSD, Hu M, Katz SG, and Wang S (2020). Multiplexed imaging of nucleome architectures in single cells of mammalian tissue. Nat. Commun. 11, 2907. 10.1038/s41467-020-16732-5. [PubMed: 32518300]

92. Horzum U, Ozdil B, and Pesen-Okvur D (2014). Step-by-step quantitative analysis of focal adhesions. MethodsX 1, 56–59. 10.1016/j.mex.2014.06.004. [PubMed: 26150935]

93. Bolte S, and Cordelières FP (2006). A guided tour into subcellular co-localization analysis in light microscopy. J. Microsc. 224, 213–232. 10.1111/j.1365-2818.2006.01706.x. [PubMed: 17210054]

94. Stewart JM, Li S, Tang AA, Klocke MA, Gobry MV, Fabrini G, Di Michele L, Rothemund PWK, and Franco E (2024). Modular RNA motifs for orthogonal phase separated compartments. Nat. Commun. 15, 6244. 10.1038/s41467-024-50003-x. [PubMed: 39080253]

95. Ingolia NT, Ghaemmaghami S, Newman JRS, and Weissman JS (2009). Genome-wide analysis in vivo of translation with nucleotide resolution using ribosome profiling. Science 324, 218–223. 10.1126/science.1168978. [PubMed: 19213877]

96. Tutucci E, Vera M, Biswas J, Garcia J, Parker R, and Singer RH (2018). An improved MS2 system for accurate reporting of the mRNA life cycle. Nat. Methods 15, 81–89. 10.1038/nmeth.4502. [PubMed: 29131164]

97. Wu B, Miskolci V, Sato H, Tutucci E, Kenworthy CA, Donnelly SK, Yoon YJ, Cox D, Singer RH, and Hodgson L (2015). Synonymous modification results in high-fidelity gene expression of

repetitive protein and nucleotide sequences. Genes Dev. 29, 876–886. 10.1101/gad.259358.115. [PubMed: 25877922]

98. Ershov D, Phan MS, Pylvänäinen JW, Rigaud SU, Le Blanc L, Charles-Orszag A, Conway JRW, Laine RF, Roy NH, Bonazzi D, et al. (2022). TrackMate 7: integrating state-of-the-art segmentation algorithms into tracking pipelines. Nat. Methods 19, 829–832. 10.1038/s41592-022-01507-1. [PubMed: 35654950]
99. Carisey A, Stroud M, Tsang R, and Ballestrem C (2011). Fluorescence recovery after photobleaching. Methods Mol. Biol. 769, 387–402. 10.1007/978-1-61779-207-6_26. [PubMed: 21748690]
100. Deakin NO, Ballestrem C, and Turner CE (2012). Paxillin and Hic-5 interaction with vinculin is differentially regulated by Rac1 and RhoA. PLoS One 7, e37990. 10.1371/journal.pone.0037990. [PubMed: 22629471]
101. Lavelin I, Wolfenson H, Patla I, Henis YI, Medalia O, Volberg T, Livne A, Kam Z, and Geiger B (2013). Differential effect of actomyosin relaxation on the dynamic properties of focal adhesion proteins. PLoS One 8, e73549. 10.1371/journal.pone.0073549. [PubMed: 24039980]

Highlights

- Hundreds of mRNAs localize to focal adhesions (FAs)
- G3BP1 also localizes to FAs and interacts with FA proteins in an RNA-dependent manner
- Removal of G3BP1 reduces FA protein mobility, FA size, and individual cell migration speed
- G3BP1's RNA-binding and dimerization domains are required for cell migration

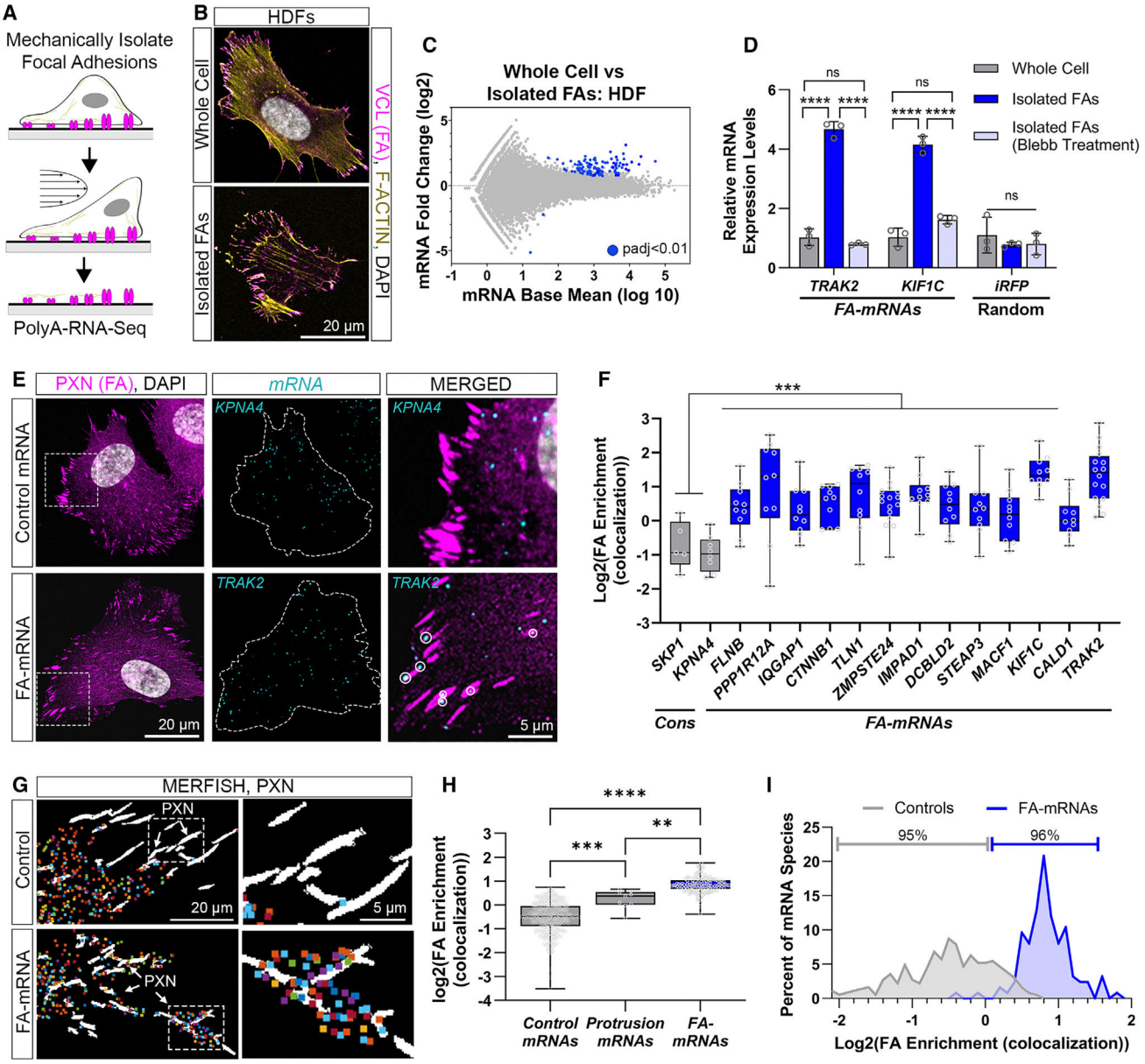

Figure 1. A distinct subpopulation of mRNAs is localized to FAs

(A) Schematic of focal adhesion (FA) isolation protocol for poly(A) RNA sequencing (poly(A)-RNA-seq).

(B) Representative images of HDFs before and after FA isolation. Cells were stained for F-ACTIN (phalloidin, yellow), vinculin (VCL; magenta), and DAPI (white).

(C) mRNA-seq results for whole cells vs. isolated FAs in HDFs. Data are plotted as log10 average expression vs. log2 fold change with $p$adj < 0.01 (determined using DESeq) for significantly localized mRNAs with four independent replicates per group.

(D) RT-qPCR for FA-mRNAs (*TRAK2* and *KIF1C*) or ectopically expressed iRFP from whole cells, isolated FAs, or isolated FAs in cells treated with blebbistatin (Blebb; 25 µM for 30 min) (two-way ANOVA with multiple comparisons, $p < 0.0001$ or $p > 0.05$ for all comparisons, $n = 3$ replicates per group, mean ± SD).

(E) Representative images of *KPNA4* or *TRAK2* (cyan) and an FA counterstain (PXN, magenta) in HDFs. Dotted outlines in mRNA images represent the outline of the cell. Dotted boxes in FA images represent the region highly magnified on the right. Solid circles represent mRNA directly on top of FA in the highly magnified images.
(F) Log2 of FA enrichment for mRNA foci directly on top of FA (co-localization) for non-localized (*SKP1* and *KPNA4*) and FA-localized mRNA in HDFs (n = 10–20 cells for all mRNAs, individual two-way unpaired t tests were used to determine significance between *SKP1* or *KPNA4* and all other mRNAs, $p < 0.001$).
(G) Composite MERFISH images of control mRNAs or FA-mRNAs (colored dots) after all hybridization rounds with FAs marked by PXN (white arrows) in HDFs. Dotted boxes in the images represent the regions highly magnified.
(H) Boxplots of log2 of FA enrichment for mRNA foci directly on top of FA (co-localization) for the control mRNA, protrusion mRNA, or FA-mRNA determined by MERFISH (one-way ANOVA with multiple comparisons, $p = 0.003$ control vs. protrusion mRNA, $p < 0.0001$ control vs. FA-mRNA, and $p = 0.0063$ protrusion vs. FA-mRNA).
(I) Histogram of log2 of FA enrichment for mRNA foci directly on top of FA (co-localization) for the control or FA-mRNA MERFISH libraries (n = 136 control mRNA and n = 122 FA-mRNA species averaged across independent experiments; control, n = 3 experiments, n = 486 cells; FA-mRNA, n = 4 experiments, n = 617 cells). 96% of FA-mRNAs have more enrichment than 95% of control mRNAs.
See also Figure S1 and Tables S2 and S3.

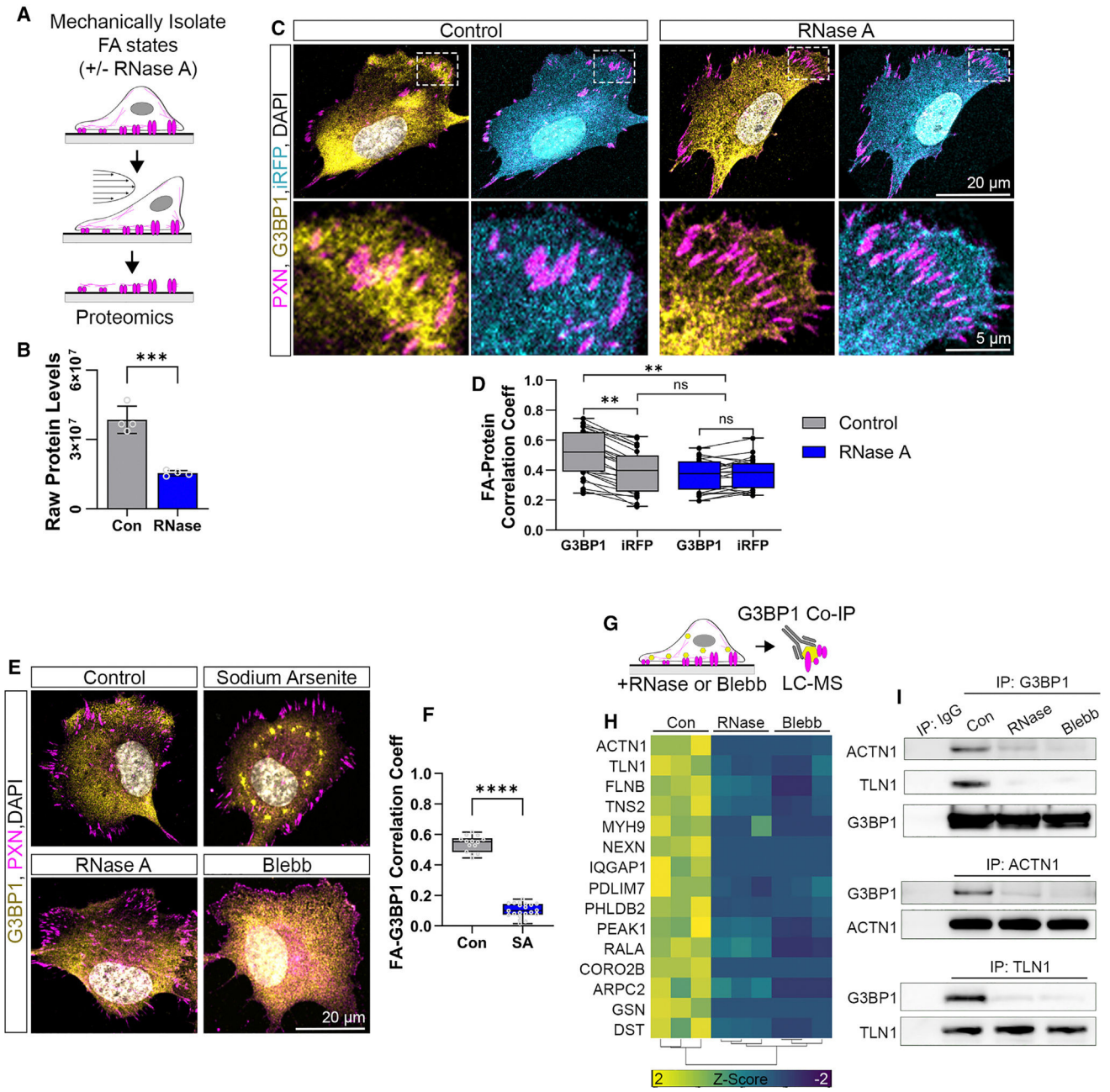

Figure 2. G3BP1 co-localizes and interacts with FA proteins in an RNA-dependent manner

(A) Schematic of FA isolation protocol using untreated or RNase A-treated HDFs (1 mg/mL for 10 min).

(B) Expression of G3BP1 with RNase A treatment from proteomics analysis of FA isolates from control or RNase A-treated HDFs (mean ± SD, two-way unpaired t test, $p = 0.0003$, $n = 4$ independent replicates).

(C) Representative image of G3BP1 (yellow) and iRFP (cyan) within control or RNase A-treated cells (1 mg/mL for 10 min) co-stained with PXN (magenta) and DAPI (white). Dotted boxes in the left images represent the highly magnified region along the bottom.

(D) Boxplots of FA-G3BP1 or FA-iRFP correlation coefficient from control or RNase A-treated cells. Paired measurements from G3BP1 and iRFP are from the same cells (two-way ANOVA with multiple comparisons, Con G3BP1 vs. Con iRFP $p = 0.0088$, vs. RNase G3BP1 $p = 0.0005$, and vs. RNase iRFP $p = 0.0016$; $n = 25$ cells).
(E) Representative images of G3BP1 (yellow) and PXN (magenta) from cells treated with RNase A (1 mg/mL for 10 min), Blebb (25 μM for 30 min), or sodium arsenite (SA; 500 μM for 45 min).
(F) Boxplots of FA-G3BP1 correlation coefficient from control or SA-treated cells (two-way unpaired t test, $p < 0.0001$, $n = 14–21$ cells).
(G) Schematic of sample preparation for G3BP1 co-immunoprecipitation (coIP) for liquid chromatography-mass spectrometry (LC-MS). Cells were treated with RNase A (1 mg/mL for 10 min) or Blebb (25 μM for 30 min) before being lysed for coIP.
(H) Heatmap of FA proteins lost or with decreased binding to G3BP1 following treatment ($n = 3$ biological replicates).
(I) Western blots of coIP samples of G3BP1, ACTN1, TLN1, or immunoglobulin (Ig)G controls for control or treated cells. Samples were treated under the same conditions as the LC-MS screen.
See also Figure S2 and Tables S3 and S4.

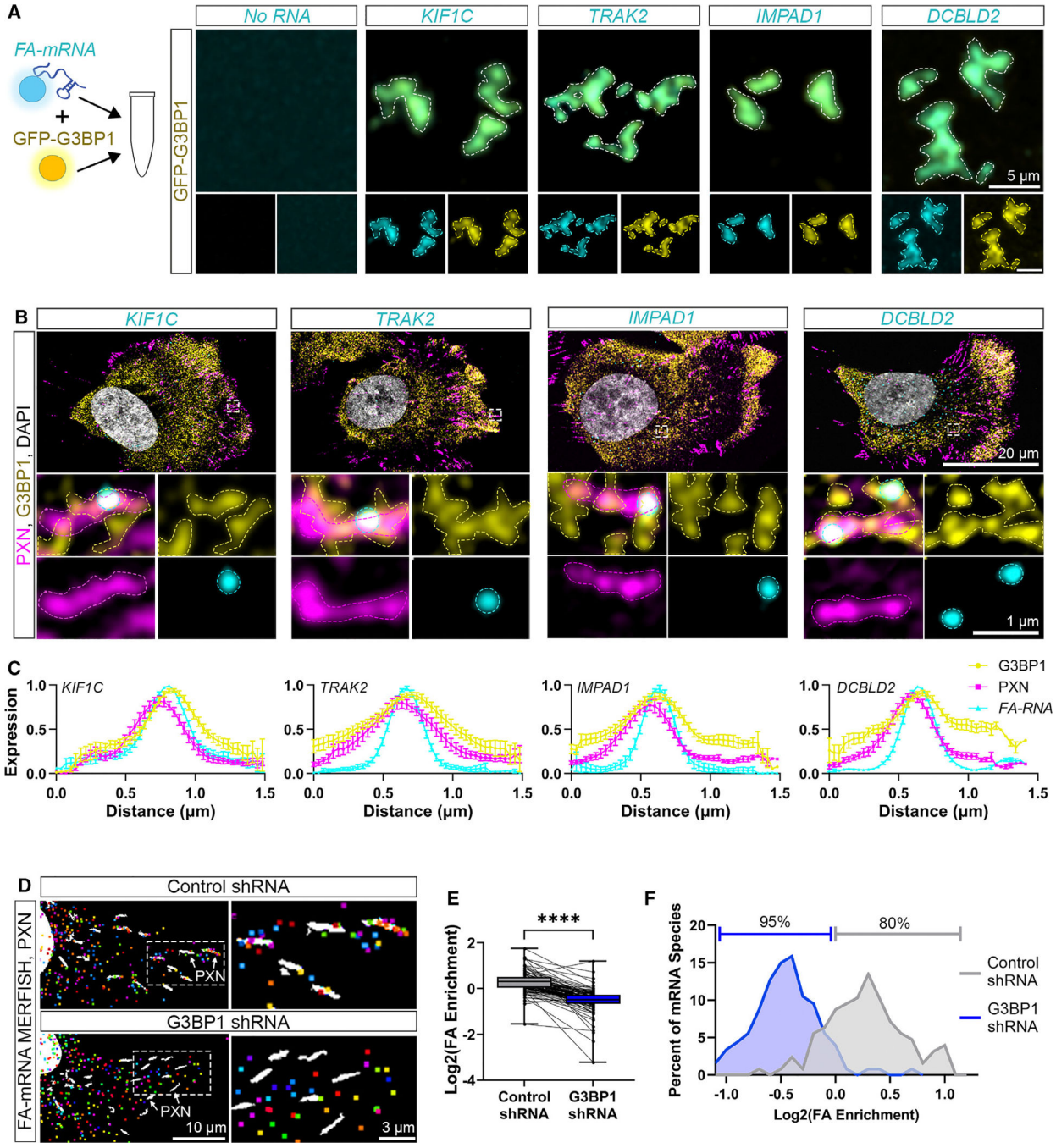

Figure 3. G3BP1 forms RNPs with FA-mRNA and is required for the enrichment of these mRNAs at FAs

(A) Schematic and confocal images of GFP-G3BP1 protein (10 μM, yellow) mixed with *in-vitro*-transcribed mRNAs (50 nM, cyan). Dotted lines represent the outlines of the G3BP1 RNP complexes.

(B) High-resolution confocal images of HDFs after immunofluorescence staining of G3BP1 (yellow) and paxillin (PXN; magenta) and smFISH of endogenous mRNA (*TRAK2*, *KIF1C*, *DCBLD2*, and *IMPAD* in cyan). Dotted lines represent outlines of proteins and mRNA. Dotted boxes in whole-cell images represent the region highly magnified along the bottom.

(C) Normalized (to max intensity) profiles of G3BP1, PXN, and mRNA fluorescent intensities averaged across multiple FAs for mRNA directly co-localizing with FAs (mean ± SD, $n = 20$ mRNA/protein complexes, two-tailed correlation matrix for each mRNA vs. G3BP1 and PXN, where $p < 0.0001$ for all Pearson correlation coefficients where r = 0.849–0.947).

(D) Composite MERFISH images for FA-mRNAs after all hybridization rounds with FAs marked by PXN (white arrows) in HDFs with a G3BP1 or control shRNA.

(E and F) Boxplot (E) and histogram (F) of log2 of FA enrichment for FA-mRNAs determined by MERFISH in G3BP1 or control shRNA-treated HDFs ($n = 122$ FA-mRNA species averaged across 3 or 4 independent experiments, $p < 0.0001$, two-way paired t test). See also Figures S3 and S4 and Table S2.

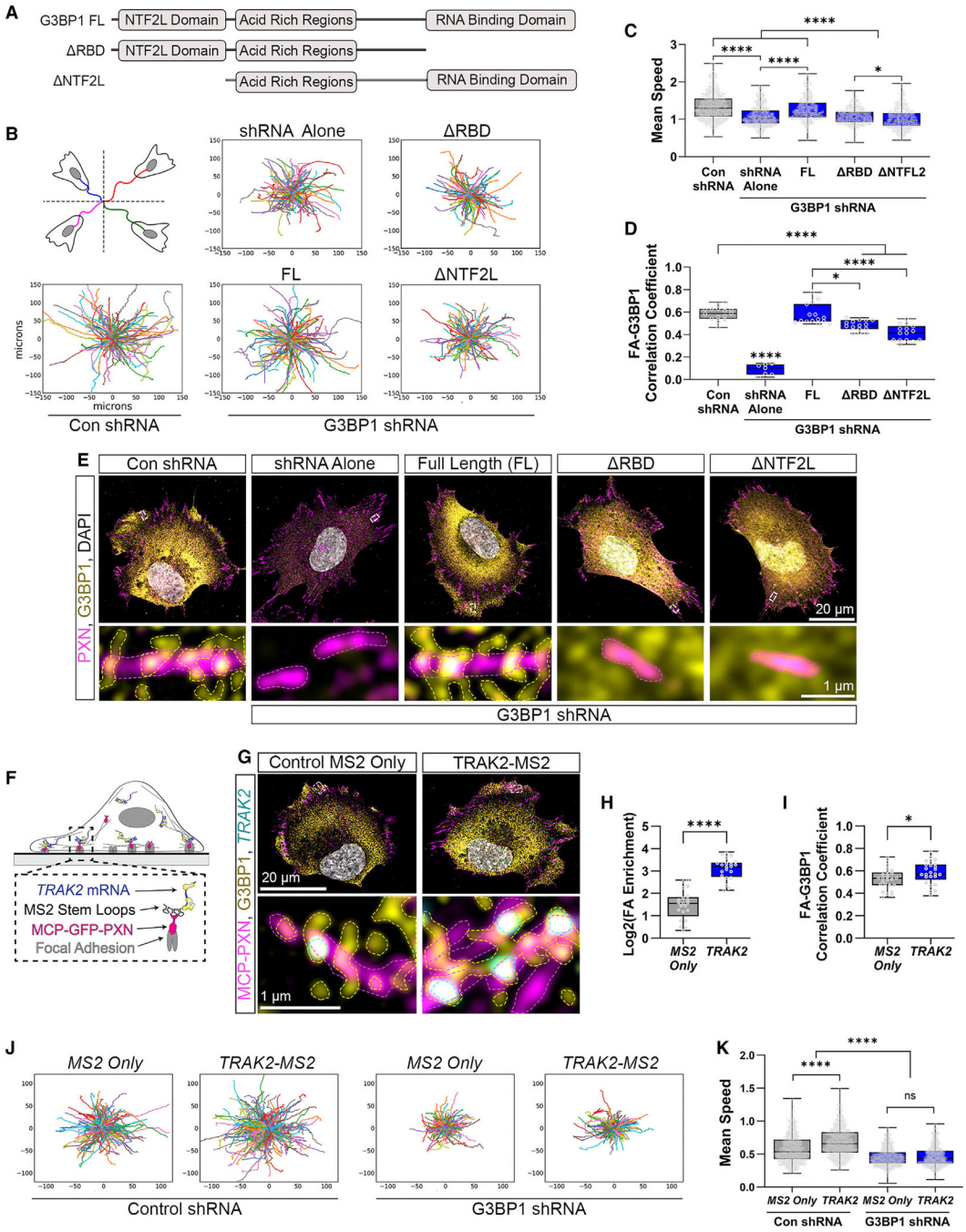

Figure 4. G3BP1 regulates individual cell migration through its function as an RNP

(A) Schematic of G3BP1 protein domains and mutants used.

(B and C) Rose plots (B) and quantification of speed (μm/min), represented as boxplots, (C) from individually migrating cells from control or G3BP1 shRNA-treated cells with either no G3BP1, full-length (FL), ΔRBD, or ΔNTF2L re-expression (one-way ANOVA with multiple comparisons, $p < 0.0001$ for Con or FL vs. shRNA alone, ΔRBD, or ΔNTF2L, and $p = 0.0445$ for ΔRBD vs. ΔNTF2L; $n = 247–346$ cells per group).

(D) Boxplots of FA-G3BP1 correlation coefficient from control or re-expression cells in E (one-way ANOVA with multiple comparisons, $p < 0.0001$ for G3BP1 shRNA only vs. all other comparisons, for Con shRNA vs. ΔRBD or ΔNTF2L, or FL vs. ΔNTF2L; $p = 0.0115$ for FL vs. ΔRBD; $n = 15$ for all groups, but $n = 7$ for G3BP1 shRNA alone).
(E) Representative images of G3BP1 (yellow) and PXN (magenta) in control or G3BP1 shRNA-treated cells with G3BP1 re-expression. Dotted lines represent outlines of proteins. Dotted boxes in the whole-cell image represent the region highly magnified along the bottom below.
(F) Schematic of MS2-MCP-GFP-PXN system. TRAK2-MS2-tagged mRNA was co-expressed with an MCP-GFP-PXN fusion protein to directly link RNA to FAs.
(G) Representative images of G3BP1 RNP complexes (yellow) and TRAK2-MS2 (cyan) in HDFs co-expressing MCP-GFP-PXN, which is incorporated into the FAs (magenta). Dotted lines represent outlines of protein/mRNA. Dotted boxes in images represent the highly magnified regions below.
(H) Quantification of smFISH images taken of cells expressing MCP-GFP-PXN and either MS2 alone or TRAK2-MS2. Boxplots represent the log2 of FA enrichment for mRNA foci directly on top of FA (co-localization) (two-way unpaired t test, $p < 0.0001$, $n = 21$ cells).
(I) Boxplots of FA-G3BP1 correlation coefficient from MS2-only- or TRAK2-MS2-expressing cells (two-way unpaired t test, $p = 0.0472$, $n = 25$ cells).
(J and K) Rose plots (microns) (J) and quantification of speed (μm/min), represented as boxplots, (K) from individually migrating cells from control or G3BP1 shRNA-treated cells with either MS2 only or TRAK2-MS2 (one-way ANOVA with multiple comparisons, $p < 0.0001$ for MS2 only vs. TRAK2-MS2 Con shRNA and MS2 only or TRAK2-MS2 Con shRNA vs. both G3BP1 shRNA groups; $n = 498–755$ cells/group).
See also Figure S5 and Videos S2, S3, S4, S5, S6, S7, S8, S9, and S10.

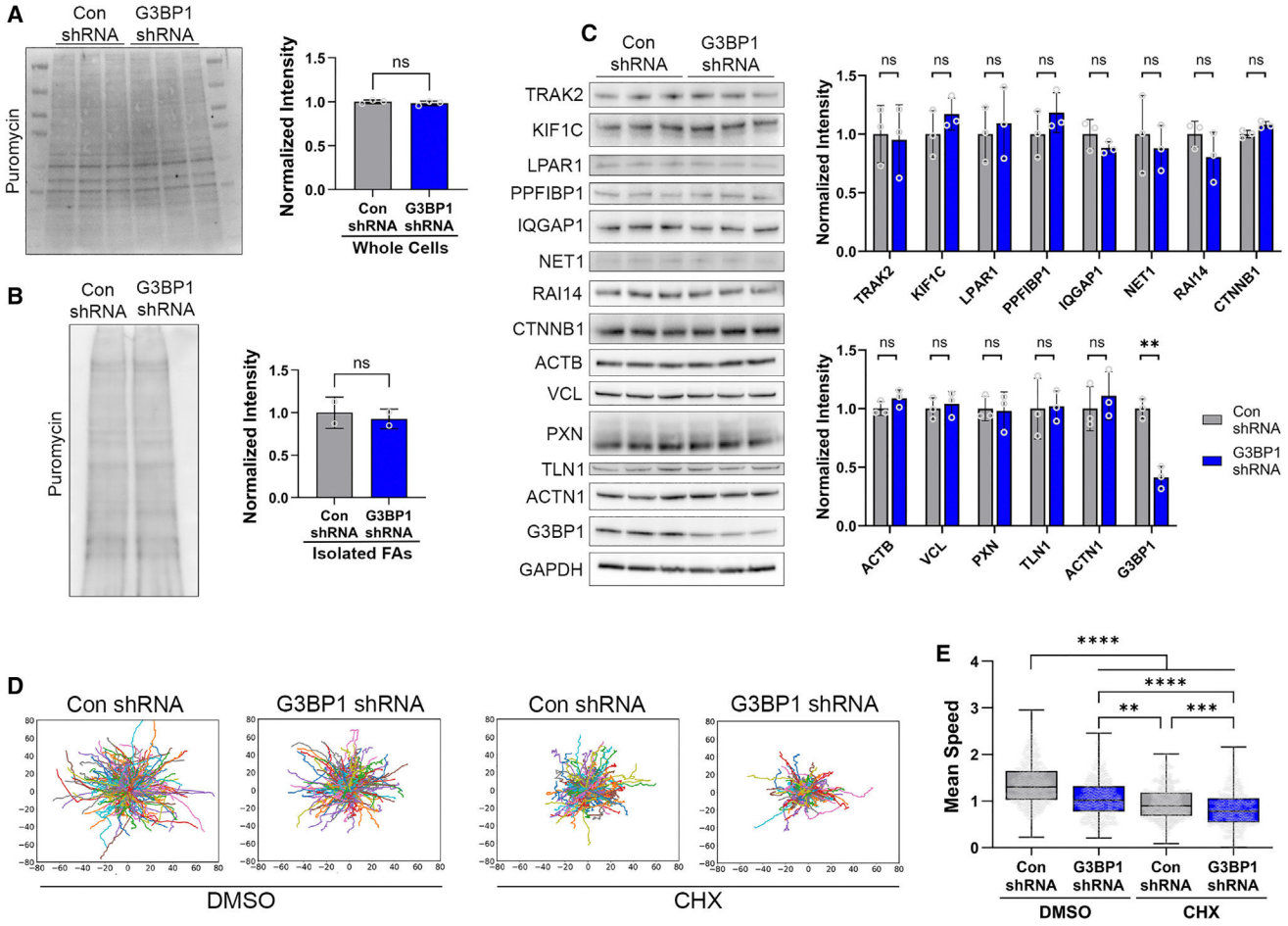

Figure 5. Analysis of protein abundance with loss of G3BP1

(A and B) Western blot images and quantification of puromycin incorporation after 5 min of puromycin treatment (5 μM) in (A) whole cells or (B) isolated FAs from control or G3BP1 shRNA-treated cells. Puromycin intensity was normalized to total protein visualized via ponceau S staining (see Figures S6A and S6B) (mean ± SD, two-way unpaired t test, $p = 0.4024$ with $n = 3$ replicates for whole cells, $p = 0.6837$ with $n = 2$ replicates [4 pooled dishes for each replicate] for isolated FAs).

(C) Western blot images and quantification for FA-mRNA encoding proteins (TRAK2, KIF1C, LPAR1, PPFIBP1, IQGAP1, NET1, RAI14, and CTNNB1), FA/cytoskeletal proteins (ACTB, VCL, PXN, TLN1, and ACTN1), or G3BP1 in Con shRNA or G3BP1 shRNA-treated cells. Protein intensity was normalized to GAPDH (mean ± SD, two-way unpaired t tests for all, $n = 3$ replicates, $p > 0.05$ for all comparisons except for G3BP1, where $p = 0.0014$).

(D and E) Rose plots (D) and quantification of speed (μm/min), represented as boxplots, (E) from individually migrating cells from control or G3BP1 shRNA-treated cells with either DMSO or CHX (100 μg/mL added at the start of imaging and continued for the 2-h video acquisition)[10] (one-way ANOVA with multiple comparisons, $p < 0.0001$ for all comparisons except for Con shRNA CHX vs. G3BP1 shRNA DMSO [$p = 0.0023$] and Con shRNA CHX vs. G3BP1 shRNA CHX [$p = 0.0008$]; $n = 284–382$ cells per group).

See also Figure S6 and Videos S11, S12, S13, and S14.

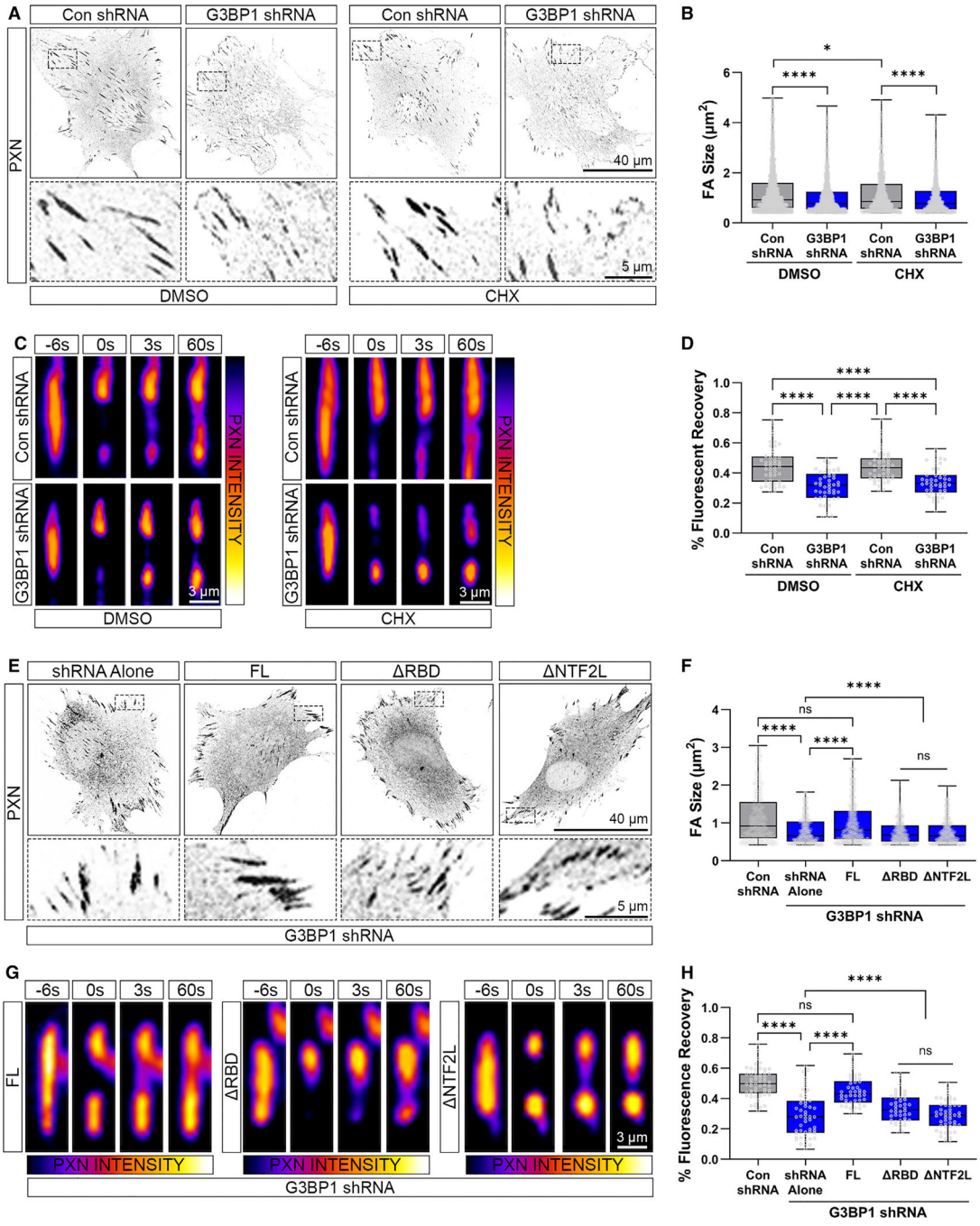

Figure 6. G3BP1 RNP function regulates FA size and FA protein mobility

(A and B) Representative images (A) and quantification (B) of FA size in HDF expressing a control or a G3BP1-targeting shRNA and treated with either DMSO or CHX (100 μg/mL for 1 h).[10] Quantification is represented as boxplots (two-way ANOVA with multiple comparisons, Con shRNA [DMSO or CHX] vs. G3BP1 shRNA [DMSO or CHX] $p < 0.0001$ and Con shRNA DMSO vs. Con shRNA CHX $p = 0.0316$; $n = 999–2,362$ FAs per group).

(C and D) Representative images (C) and quantification (D) of FRAP of PXN+ FAs in cells expressing a control or a G3BP1-targeting shRNA and treated with either DMSO or CHX (100 μg/mL for 1 h).[10] PXN was ectopically expressed as PXN-iRFP. Quantification is represented as boxplots (two-way ANOVA with multiple comparisons, $p < 0.0001$ for all comparisons shown and $p > 0.05$ for all other comparisons; $n = 47–49$ FA FRAPs per group).

(E and F) Representative images (E) and quantification (F) of FA size in control or G3BP1 shRNA-treated cells with either no G3BP1, full-length (FL), ΔRBD, or ΔNTF2L re-expression. Quantification is represented as boxplots (one-way ANOVA with multiple comparisons, $p < 0.0001$ for Con shRNA or FL vs. all other groups, $n = 292–480$ FA per group).

(G and H) Representative images (G) and quantification of (H) FRAP of PXN+ FAs in cells expressing a control or a G3BP1-targeting shRNA with G3BP1 re-expression. PXN was ectopically expressed as PXN-mCherry. Quantification is represented as boxplots (one-way ANOVA with multiple comparisons, $p < 0.0001$ for Con shRNA or FL vs. all other groups, $n = 46–55$ FA FRAPs per group).

See also Figure S7 and Videos S15, S16, S17, S18, S19, S20, and S21.

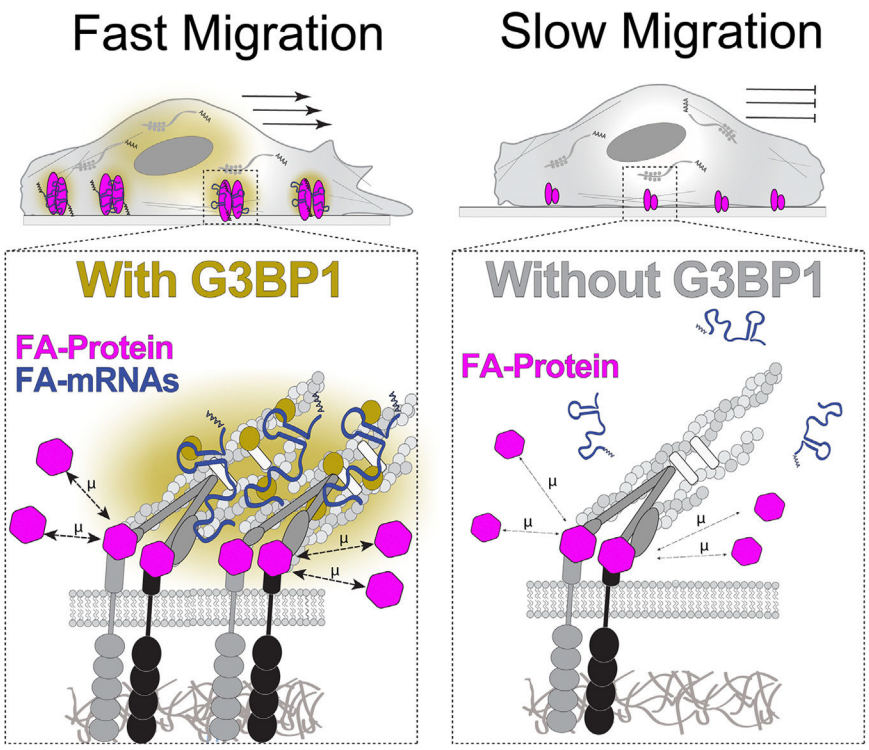

Figure 7. Proposed working model suggesting a role for G3BP1 RNPs in promoting FA protein mobility to maintain FA size and regulate cell migration speed

We demonstrate that focal adhesions (FAs) are enriched with mRNAs that have longer coding and untranslated regions, exhibit lower translation levels, and contain AU-rich elements, forming G3BP1 ribonucleoprotein (RNP) complexes essential for cell migration. In normal cells, G3BP1 localizes at FAs, and FA protein mobility is enhanced, leading to increased FA size and faster cell migration. Removing G3BP1 inhibits FA protein mobility and halts cell migration without affecting FA proteins or general protein translation. Our findings indicate that G3BP1 RNPs regulate cell migration by modulating FA protein dynamics.

KEY RESOURCES TABLE

REAGENT or RESOURCE	SOURCE	IDENTIFIER
Antibodies		
Mouse monoclonal Anti-Vinculin	MilliporeSigma	Cat# V9131; RRID: AB_477629
Rabbit monoclonal Anti-Paxillin (Y113)	Abcam	Cat# ab32084; RRID: AB_779033
Mouse monoclonal Anti-G3BP1 (H-10)	Santa Cruz	Cat# sc-365338; RRID: AB_10846950
Rabbit polyclonal Anti-IGF2BP1	MilliporeSigma	Cat# HPA021367; RRID: AB_1851480
Rabbit polyclonal Anti-G3BP2	MillporeSigma	Cat# HPA018425; RRID: AB_1849352
Rabbit polyclonal Anti-Paxillin	ThermoFisher	PA5-34910; RRID: AB_2552260
Mouse monoclonal Anti-G3BP1 (H-10)	Santa Cruz	Cat# sc-365338; RRID: AB_10846950
Mouse monoclonal Anti-α-actinin (H-2)	Santa Cruz	Cat# sc-17829; RRID: AB_626633
Mouse monoclonal Anti-Talin (8d4)	MilliporeSigma	Cat# T3287; RRID: AB_477572
Mouse monoclonal Anti-Talin1 (93E12)	Abcam	Cat# ab104913; RRID: AB_10858284
Rabbit monoclonal Anti-GAPDH (14C10)	Cell Signaling	Cat# 2118; RRID: AB_561053)
Mouse monoclonal Anti-Akt1/2/3 (5C10)	Santa Cruz	Cat# sc-81434; RRID: AB_1118808
Mouse monoclonal Anti-α-Tubulin (DM1A)	MilliporeSigma	Cat# 05-829; RRID: AB_310035
Rabbit polyclonal Anti-β-Actin (W-21)	Santa Cruz	Cat # sc-130656; RRID: AB_2223228
Mouse monoclonal Anti-PDI (C-2)	Santa Cruz	Cat# sc-74551; RRID: AB_2156462
Mouse monoclonal Anti-Puromycin (12D10)	MilliporeSigma	Cat# MABE343; RRID: AB_2566826
Mouse monoclonal Anti-Tom20 (F-10)	Santa Cruz	Cat# sc-17764; RRID: AB_628381
Rabbit polyclonal Anti-TRAK2	ThermoFisher	Cat# PA5-21858; RRID: AB_11155420
Rabbit polyclonal Anti-KIF1C	Novus Biologicals	Cat# NBP1-85978; RRID: AB_11025088
Rabbit polyclonal Anti-EDG2 (LARP1)	MilliporeSigma	Cat# SAB4500689; RRID: AB_10761250
Rabbit polyclonal Anti-PPF1BP1	MilliporeSigma	Cat# HPA001924; RRID: AB_1079665
Rabbit polyclonal Anti-IQGAP1	Abcam	Cat# ab86064; RRID: AB_1925119
Rabbit polyclonal Anti-NET1	Abcam	Cat# ab113202; RRID: AB_10863612
Rabbit polyclonal Anti-RAI14	MilliporeSigma	Cat# HPA036949; RRID: AB_10670568
Rabbit polyclonal Anti-β-Catenin	MilliporeSigma	Cat# C2206; RRID: AB_476831
Goat anti-Rabbit IgG Secondary Antibody 488	ThermoFisher	Cat# A-32731;RRID: AB_2633280
Goat anti-Rabbit IgG Secondary Antibody 647	ThermoFisher	Cat# A-21244;RRID: AB_2535812
Goat anti-Mouse IgG Secondary Antibody 488	ThermoFisher	Cat# A-11001;RRID: AB_2534069
Goat anti-Mouse IgG Secondary Antibody 647	ThermoFisher	Cat# A-21235;RRID: AB_2535804
IgG Isotype Control	ThermoFisher	Cat# 31235; RRID: AB_243593
Anti-mouse IgG, HRP-linked Antibody	Cell Signaling	Cat# 7076; RRID: AB_330924
Anti-rabbit IgG, HRP-linked Antibody	Cell Signaling	Cat# 7074; RRID: AB_2099233
Alexa Fluor™ 568 Phalloidin	ThermoFisher	A12380
Chemicals, peptides, and recombinant proteins		
Blebbistatin	MilliporeSigma	B0560
Cycloheximide	MilliporeSigma	C4859
RNase A	ThermoFisher	EN0531

REAGENT or RESOURCE	SOURCE	IDENTIFIER
Sodium arsenite	MilliporeSigma	1062771000
Triethanolamine	MilliporeSigma	90279
SYBR Green	Kapa Biosystems	KR0389
Yeast t-RNA	Life Technologies	15401011
Dextran sulfate	MilliporeSigma	D8906
Murine RNase inhibitor	NEB	M0314L
Ethylene carbonate	MilliporeSigma	E26258
Cyanine 3-UTP	Enzo Life Sciences	EZ-42505
CellTrackerTM Orange CMTMR Dye	ThermoFisher	C2927
Q5 High-Fidelity DNA Polymerase	NEB	M0491L
Lipofectamine 2000	ThermoFisher	11668019
M199 medium	ThermoFisher	11150-059
Endothelial cell growth supplement	Sigma	H3149-100KU
Penicillin-Streptomycin	ThermoFisher	15140122
Fibroblast Growth Medium	ATCC	PCS-201-030
Fibroblast Growth Kit-Low Serum	ATCC	PCS-201-041
Phenol Red (cell culture)	ATCC	PCS-999-001
DMSO	VWR	IC0219605525
TRIzol	Invitrogen	15596026
Trypsin-EDTA (0.05%), phenol red	ThermoFisher	25300054
Fibronectin bovine plasma	MilliporeSigma	F1141
Prolong Diamond Antifade with DAPI	ThermoFisher	P36971
Fluoromount-G™ Mounting Medium, with DAPI	ThermoFisher	00-4959-52
Protease Inhibitor Cocktail III	MilliporeSigma	539134
SuperSignal™ West Pico PLUS Chemiluminescent Substrate	Thermo	34580
Critical commercial assays		
QuantSeq 3'mRNA-Seq	Lexogen	191.96
RiboLace Kit	Immagina BioTECHNOLOGY	RL001
SuperScript™ IV	ThermoFisher	18090010
MS compatible Co-IP kit	ThermoFisher	90409
Pierce Classic Magnetic IP/Co-IP Kit	ThermoFisher	88804
T7 MEGAscript kit	ThermoFisher	AM1334
Gibson Assembly Master Mix	NEB	E2611
Q5® Site-Directed Mutagenesis Kit	NEB	E0554S
Deposited data		
3'RNA-Seq of HDFs, HUVECs (whole cell and isolated FAs)	This Study	GEO: GSE246955
Ribo-seq of HDFs	This Study	GEO: GSE246499
SuperSeries of all sequencing data	This Study	GEO: GSE246956
All Proteomics Data	This Study	PRIDE: PXD059392

REAGENT or RESOURCE	SOURCE	IDENTIFIER
Experimental models: Cell lines		
Human umbilical vein endothelial cells (HUVECs)	Cell Applications	200-05n
Human dermal fibroblasts (HDFs)	ATCC	PCS-201-010
Lenti-X 293T	Takara	632180
Oligonucleotides		
Control MERFISH Library (see Table S2)	This Study	N/A
FA-mRNA MERFISH Library (see Table S2)	This Study	N/A
ACTB_F - GTCATTCCAAATATGAGATGCGTTG	This Study	N/A
ACTB_R - TGCTATCACCTCCCCTGTGT	This Study	N/A
TRAK2_F - GGAACAACAGCTTGTCAGCG	This Study	N/A
TRAK2_R - CATTGTCAGTTGCCGTTGGG	This Study	N/A
KIF1C_F - ACAACGTGTGCATCTTTGCC	This Study	N/A
KIF1C_R - TCGTACCCGCTCACAGTAGA	This Study	N/A
iRFP_F - GTCGACGTCACCTATCAGCC	This Study	N/A
iRFP_R - CAGCTCGAAACGGATGAAGC	This Study	N/A
Recombinant DNA		
Lenti-PXN-mCherry	This Study	N/A
Lenti-PXN-iRFP	This Study	N/A
Lenti-MCP-GFP-PXN	This Study	N/A
Lenti-MS2 Only	This Study	N/A
Lenti-TRAK2-MS2	This Study	N/A
Lenti-ΔTRAK2-MS2	This Study	N/A
pLenti6.2_miRFP670	Addgene	113726
Lenti-FL-G3BP1-SNAP	This Study	N/A
Lenti-ΔRBD-G3BP1-SNAP	This Study	N/A
Lenti-ΔNTF2L-G3BP1-SNAP	This Study	N/A
HaloTag-bActinCDS-bActinUTR-MS2V5	Addgene	102718
HaloTag-ΔbActinCDS-bActinUTR-MS2V5	This Study	N/A
MISSION® pLKO.1-puro Non-Mammalian shRNA Control Plasmid (Con shRNA)	MilliporeSigma	SHC002
G3BP1 shRNA - CDS targeting	MilliporeSigma	SHCLNG-NM_005754; TRCN0000008723
G3BP1 shRNA - 3'UTR targeting	MilliporeSigma	SHCLNG-NM_005754; TRCN0000008719
TRAK2 shRNA - 3'UTR targeting	MilliporeSigma	SHCLNG-NM_015049; TRCN0000151916
psPAX2	Addgene	12260
pMD2.G	Addgene	12259
Lenti-osTIR1(F74G)-P2A-BFP	This Study	N/A
Lenti-G3BP1-eGFP-AID2	This Study	N/A
Software and algorithms		

REAGENT or RESOURCE	SOURCE	IDENTIFIER
Fiji	Schindelin et al.[79]	https://fiji.sc/
Mathematica 11.1	Wolfram Research Inc.	https://www.wolfram.com/mathematica/
MATLAB	MathWorks	https://www.mathworks.com/products/matlab.html
Prism	GraphPad	https://www.graphpad.com
Python 3.12	The Python Software Foundation	https://www.python.org/
LAS X	Leica	https://www.leica.com
ZEN 3.3	Zeiss	https://www.zeiss.com/microscopy/us/home.html
NIS-Elements	Nikon	https://www.microscope.healthcare.nikon.com/products/software/nis-elements
Other		
1.5# coverslips of 40-mm diameter	Bioptechs	40-1313-03193
double-sided spacer	MilliporeSigma	GBL654002
Interplak Water Jet	Conair	WJ6R/WJ6RW; B000F54AQA
Cell Lifter	LabScientific	CL-25